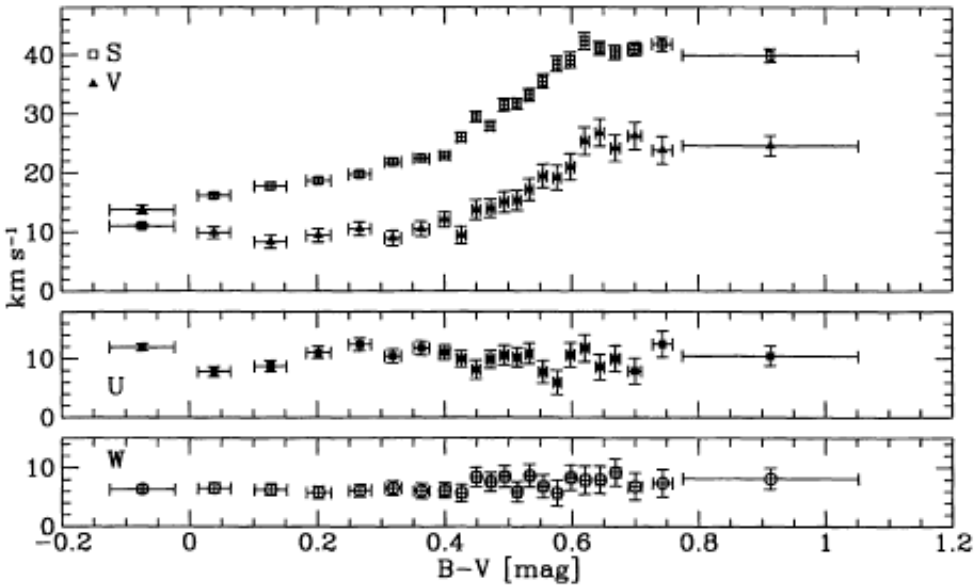

Dehnen & Binney (1998)

Figure 3. The components U, V and W of the solar motion with respect to stars with different colour $B - V$. Also shown is the variation of the dispersion S with colour.

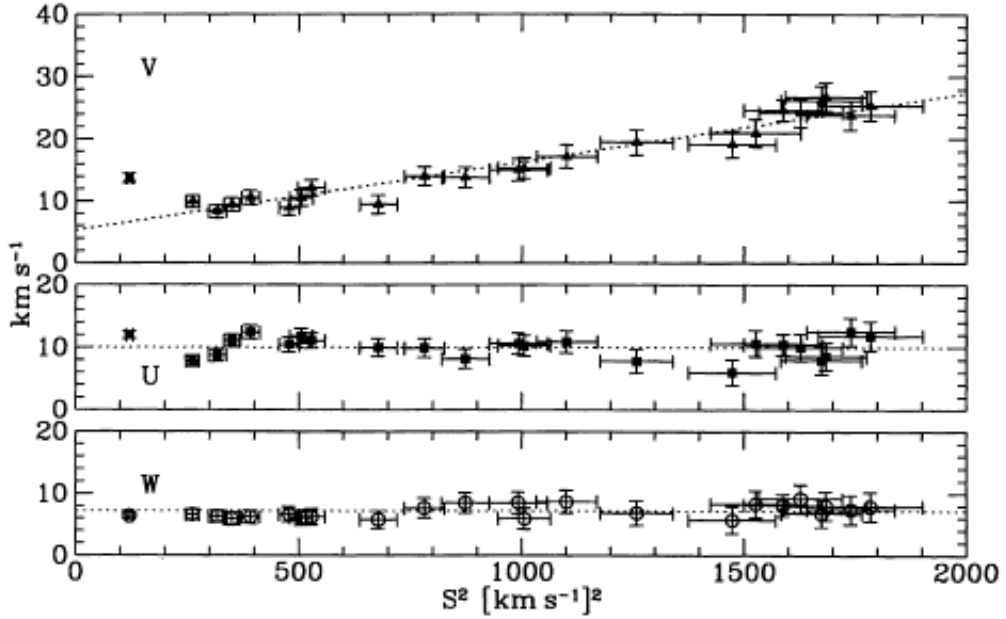

Figure 4. The dependence of U, V and W on S^2. The dotted lines correspond to the linear relation fitted (V) or the mean values (U and W) for stars bluer than $B - V = 0$.

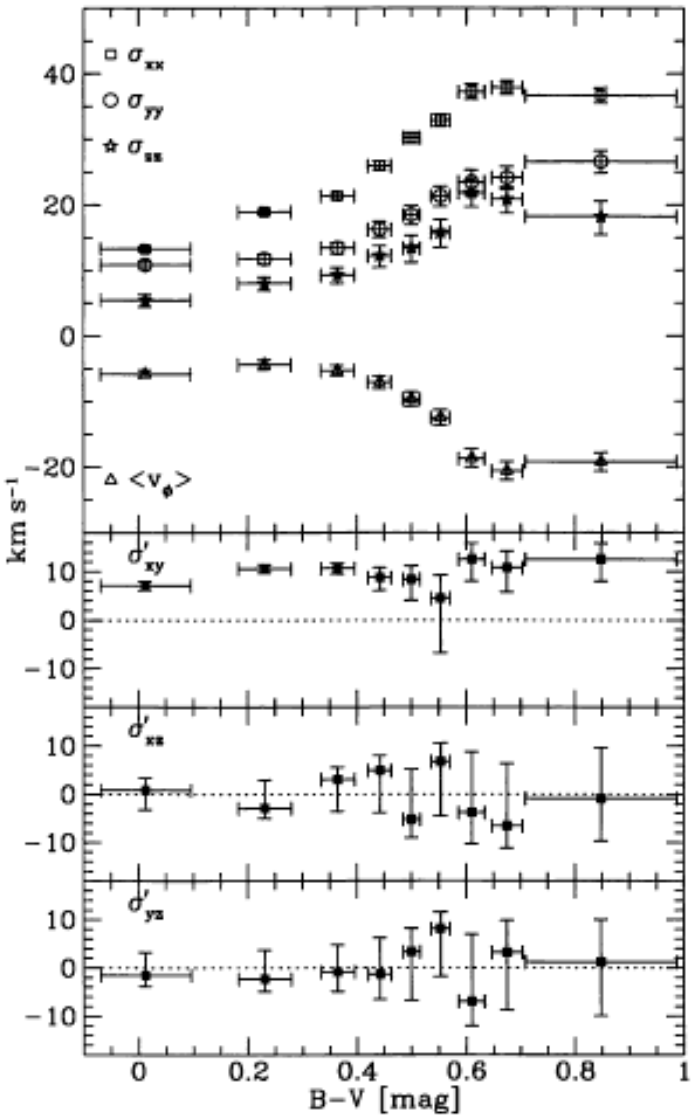

Figure 5. Velocity dispersions for stars in different colour bins. The top panel shows the mean rotation velocity (negative values imply lagging with respect to the LSR) and the three main velocity dispersions. In the three bottom panels $\sigma'_{ij} = \mathrm{sign}(\sigma^2_{ij})\,|\sigma^2_{ij}|^{1/2}$ is plotted for the mixed components of the tensor σ^2_{ij}.

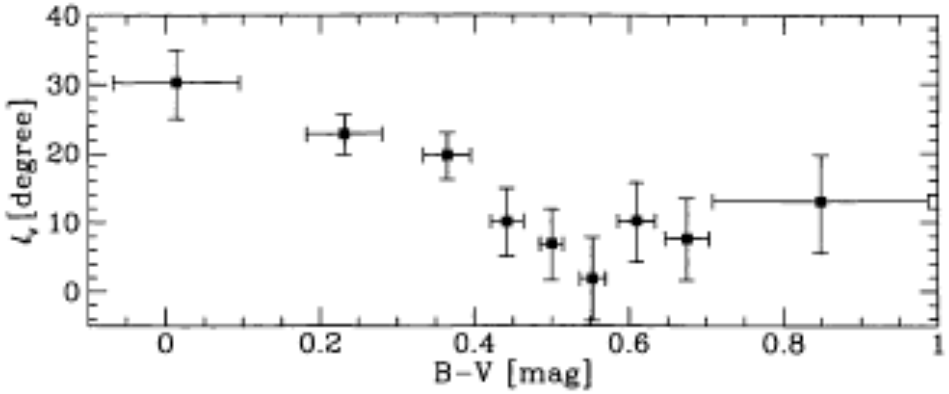

Figure 6. The vertex deviation ℓ_v versus $B-V$ colour. The error bars correspond to the 15.7 and 84.3 percentiles (i.e. 1σ error) and have been obtained assuming a multivariate Gaussian distribution in the σ^2_{ij} with variance evaluated via equation (15).

Dehnen & Binney (1998)

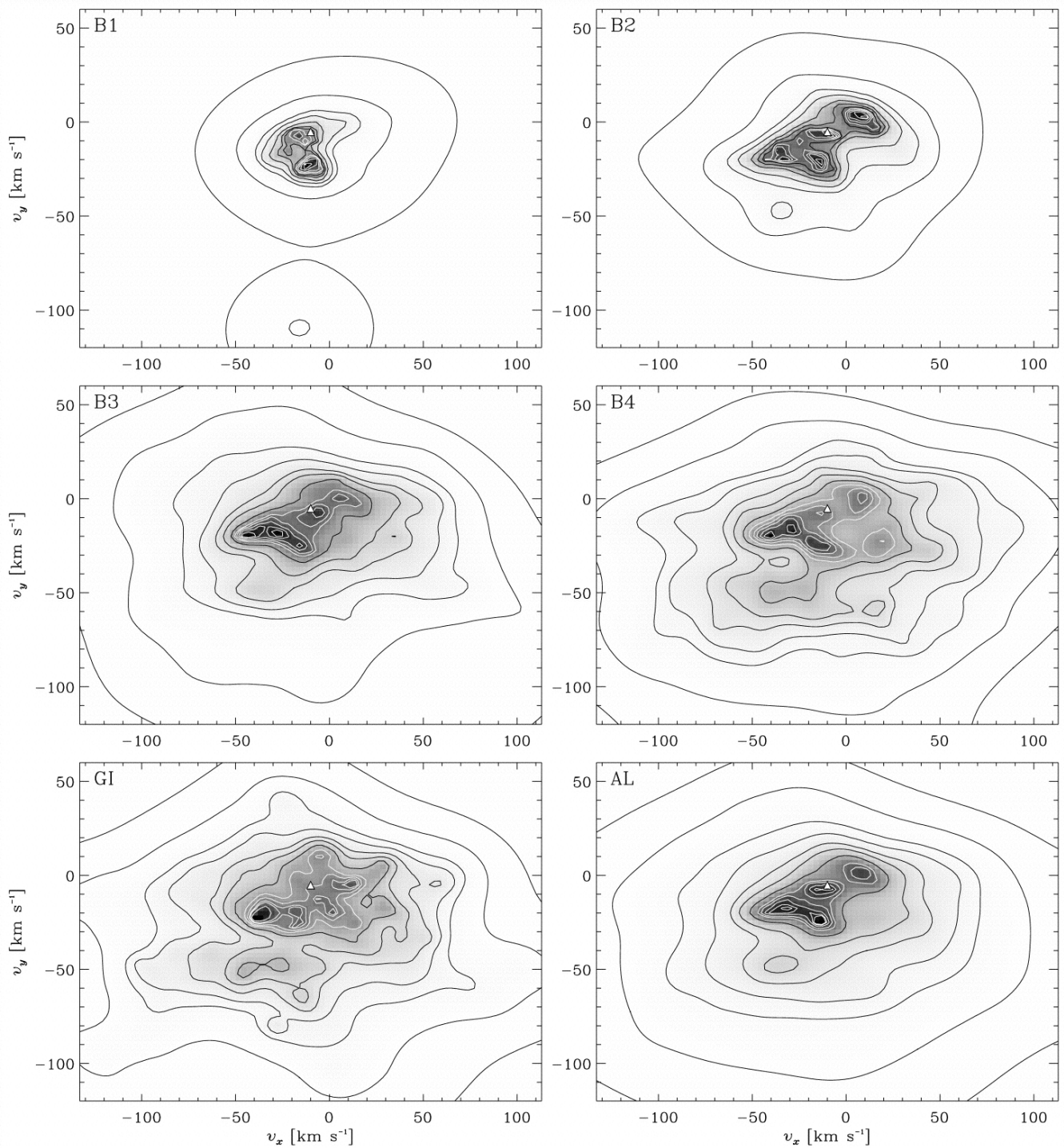

Dehnen (1998)

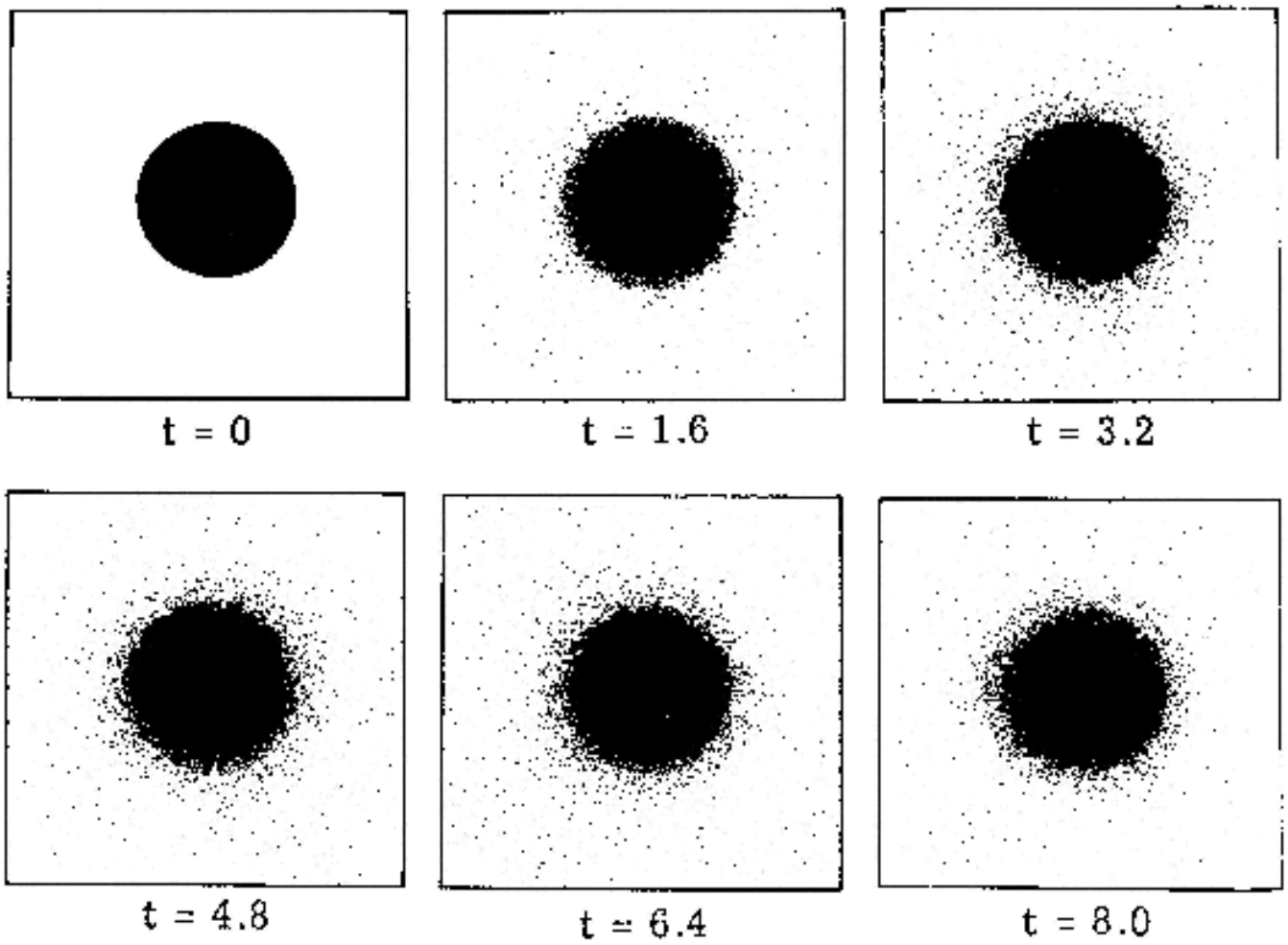

Hohl (1971)

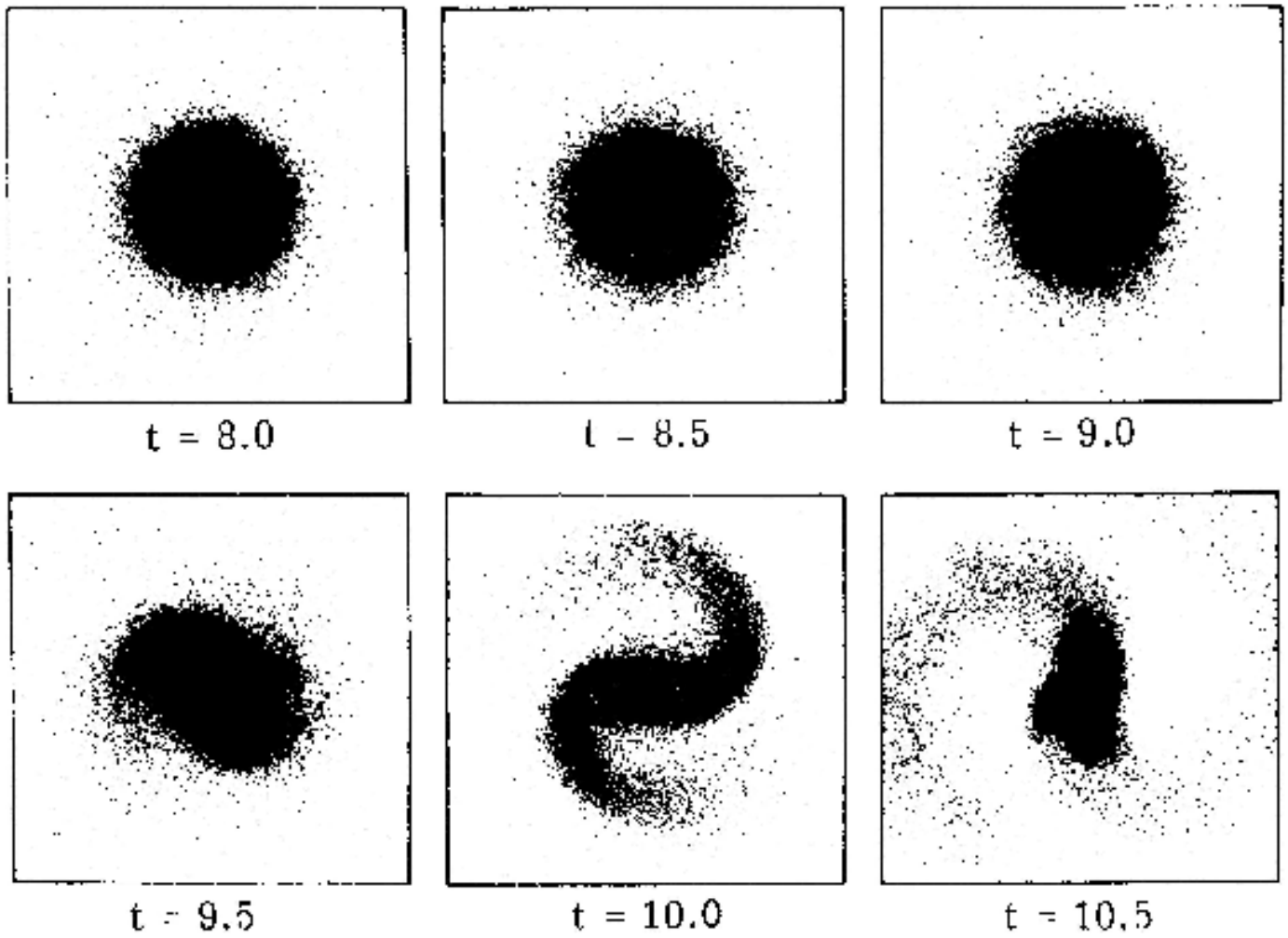

Hohl (1971)

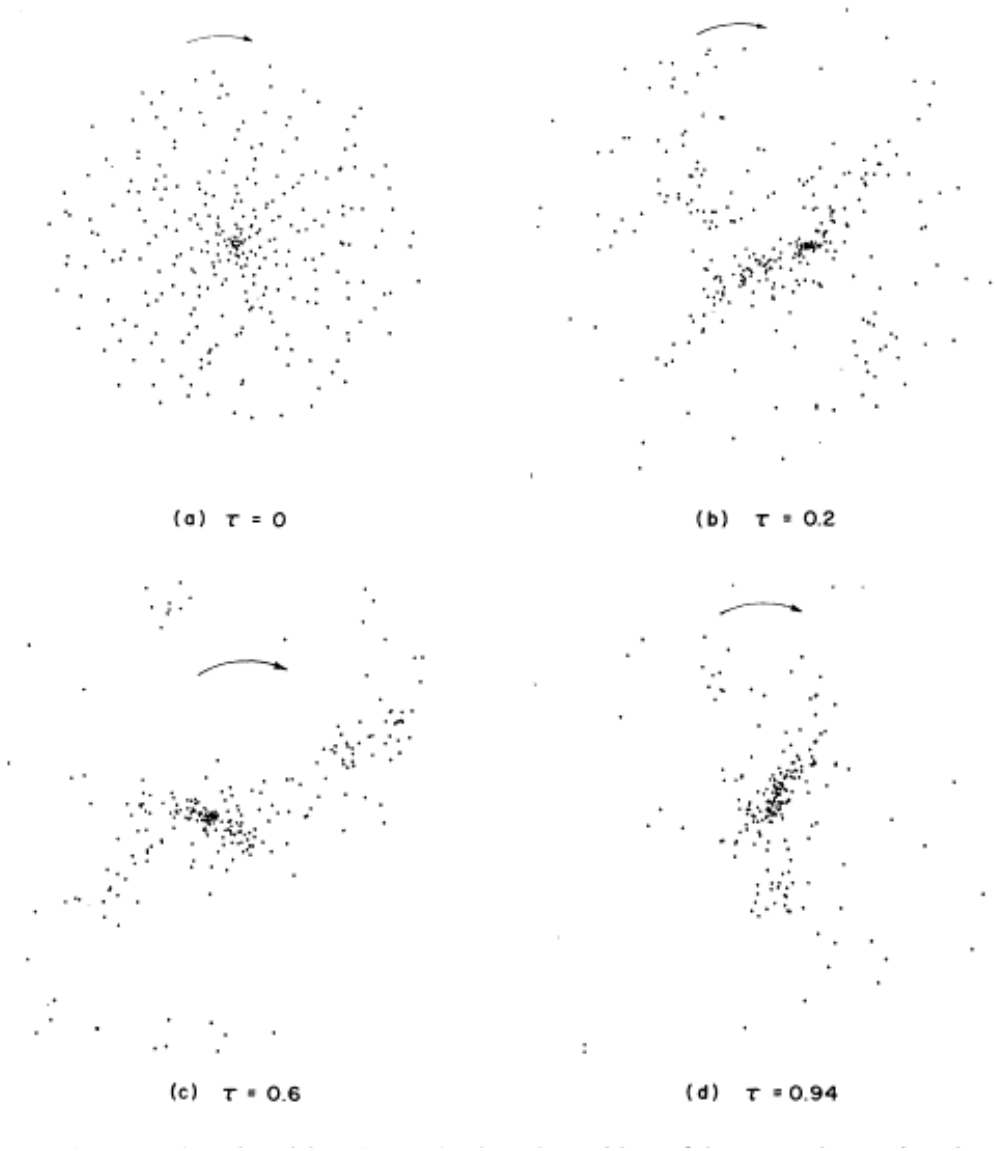

Ostriker & Peebles (1973)

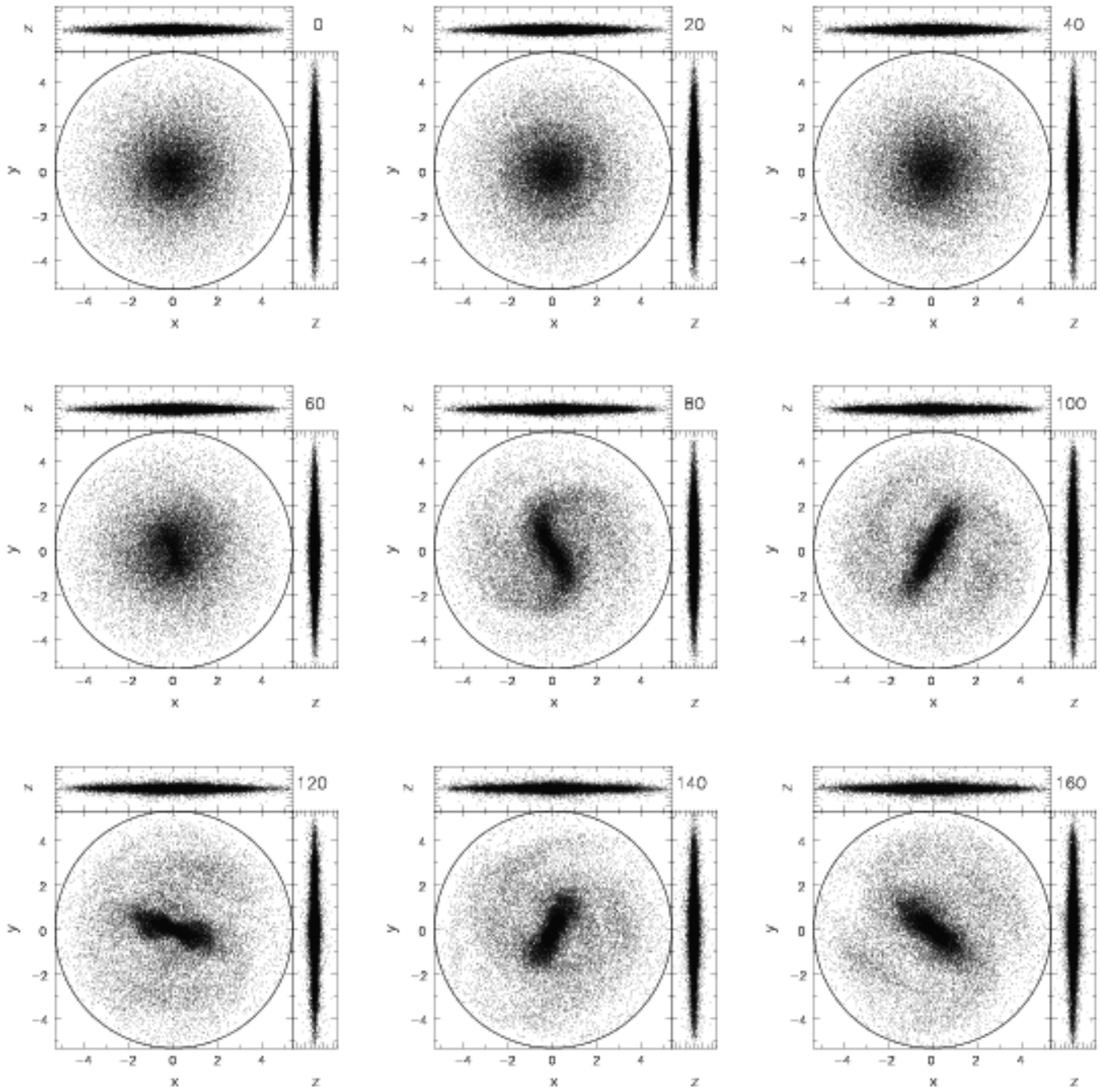

Sellwood (2005)

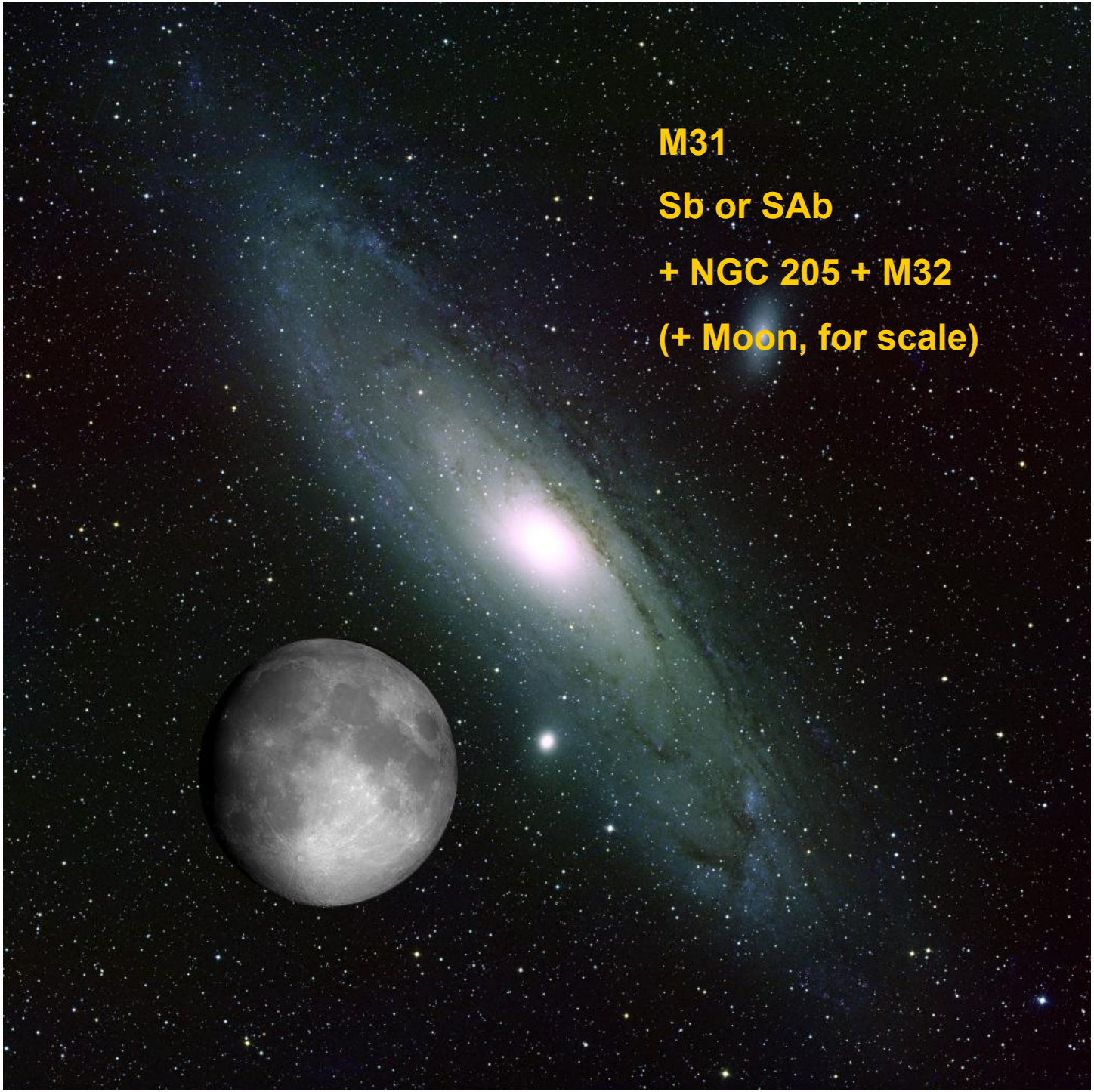
M31
Sb or SAb
+ NGC 205 + M32
(+ Moon, for scale)

NGC 1365

SBb or SB(s)b

Arm class 12 (grand design)

NGC 1300

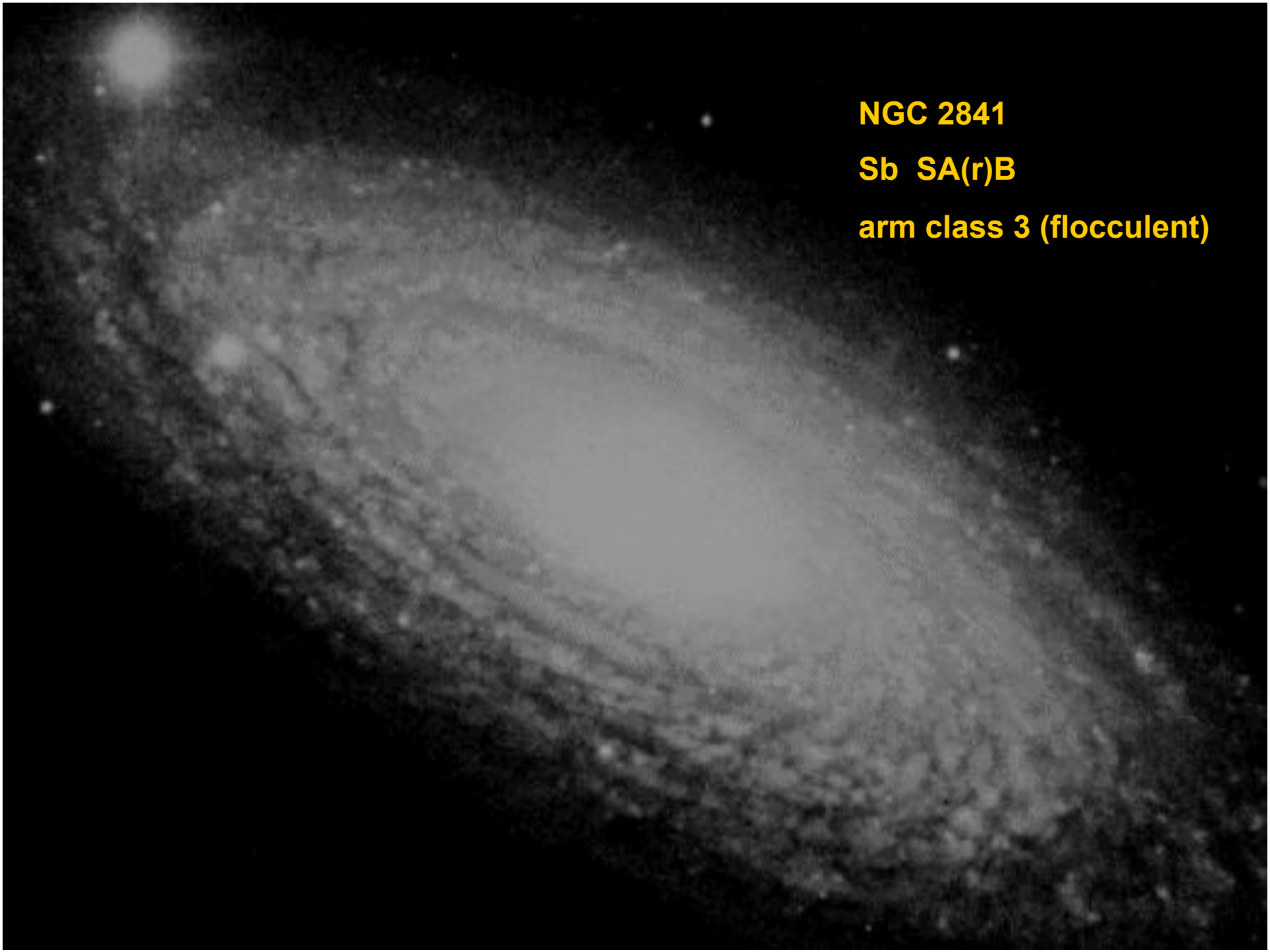
NGC 2841
Sb SA(r)B
arm class 3 (flocculent)

M100

Sbc SAB(s)bc

arm class 12 (grand design)

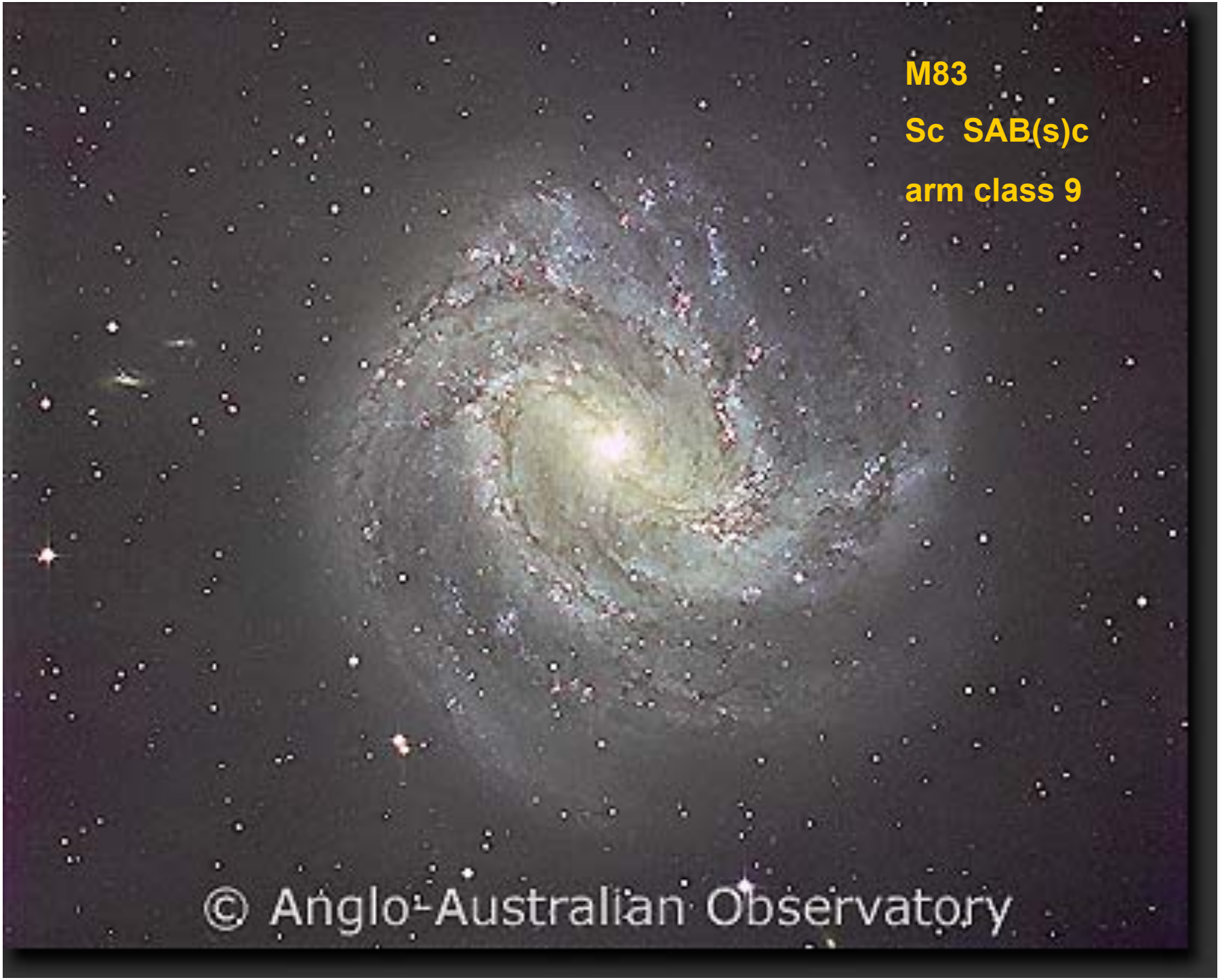
M83
Sc SAB(s)c
arm class 9
© Anglo-Australian Observatory


NGC 2997
Sc SA(s)c
arm class 9
©Anglo-Australian Observatory


M101
Scd SAB(rs)cd
arm class 9

M33

Scd SA(s)cd

arm class 5

M51

Sbc SAbc

arm class 12 (grand design)

NGC 5195

SB0(pec)

Lupton color scheme

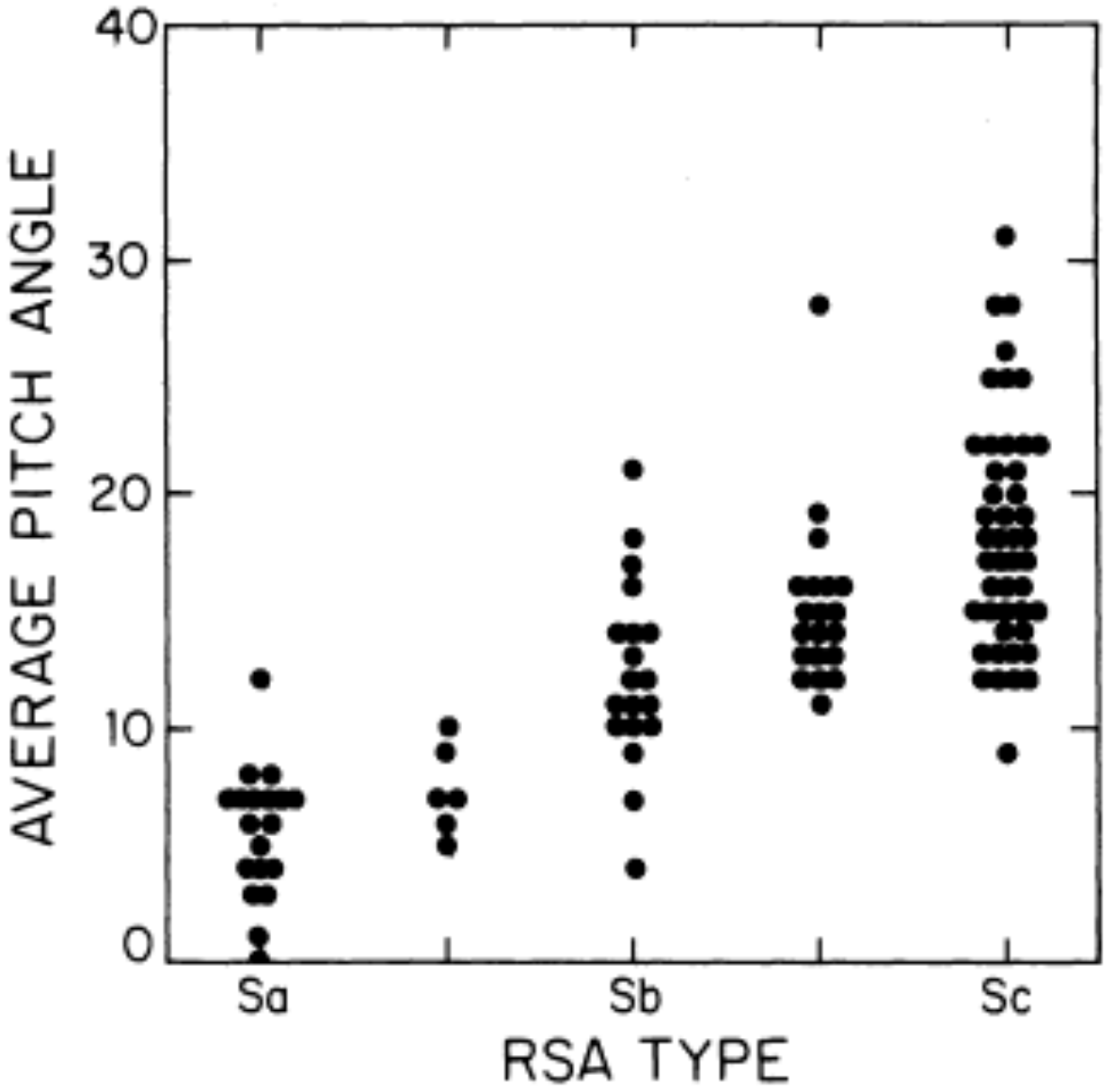

FIG. 7. Measured pitch angle vs Hubble type, the latter from Sandage and Tammann.

Kennicutt (1981)

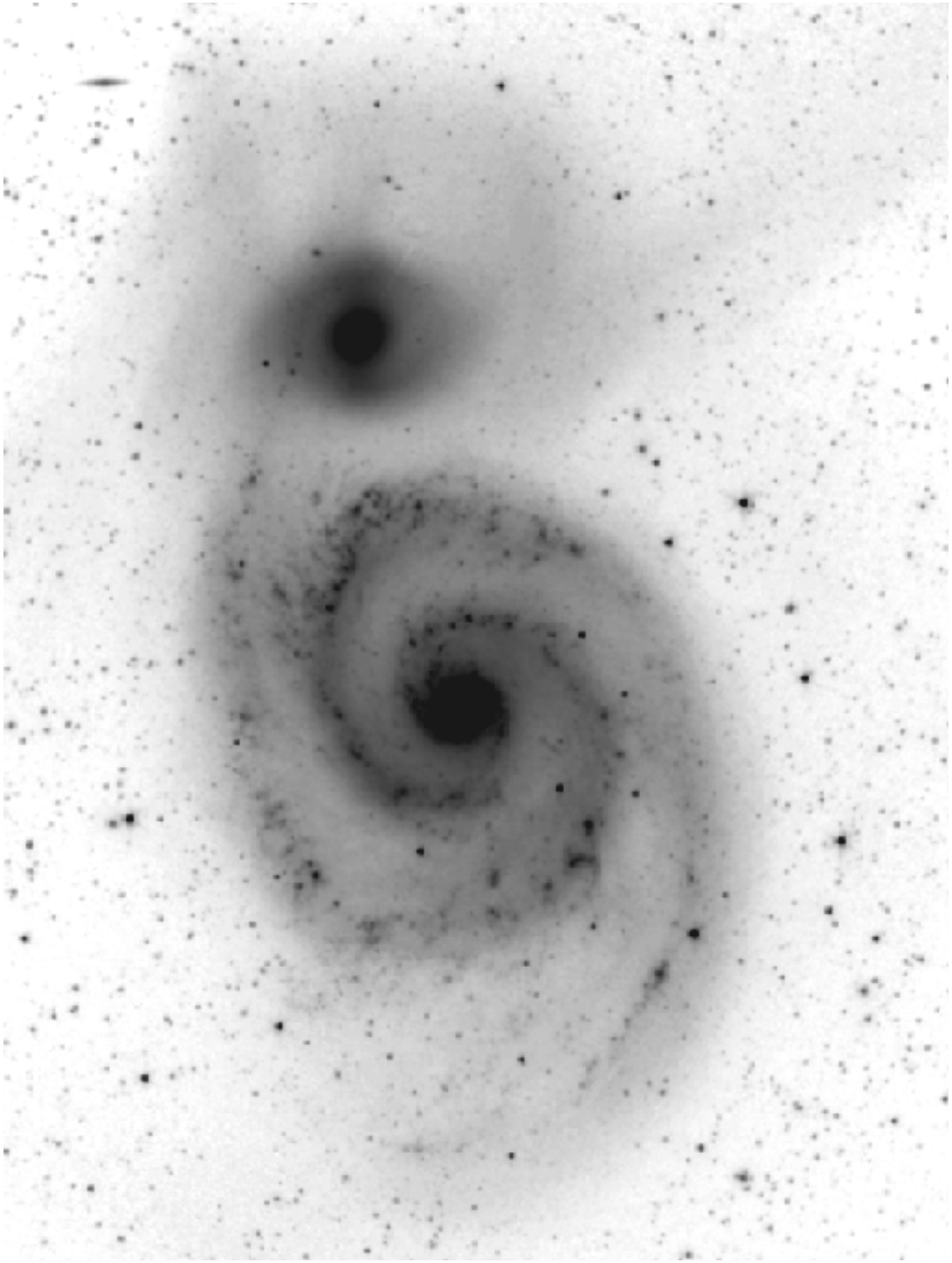

M51 – near-infrared

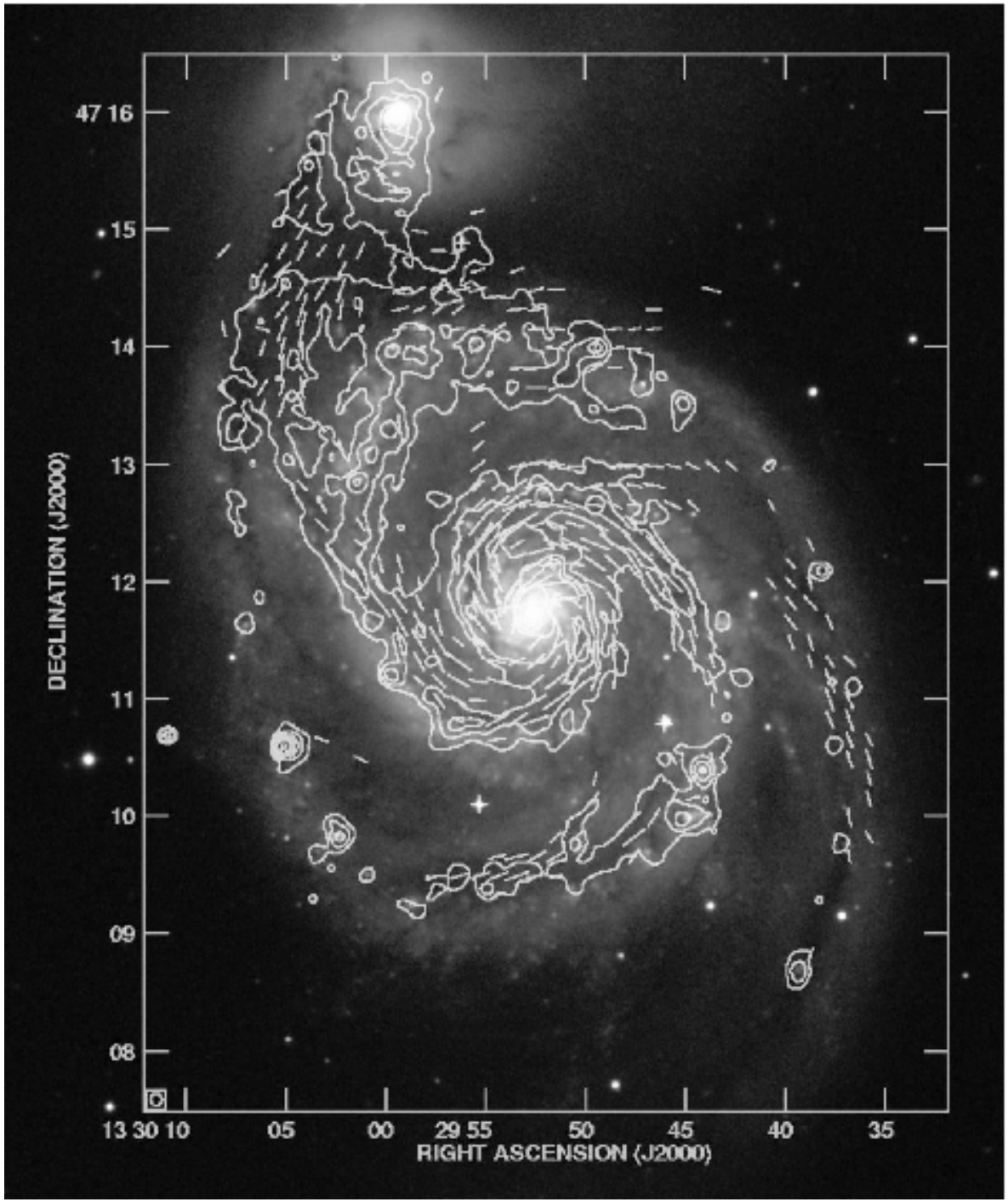

M51

radio continuum

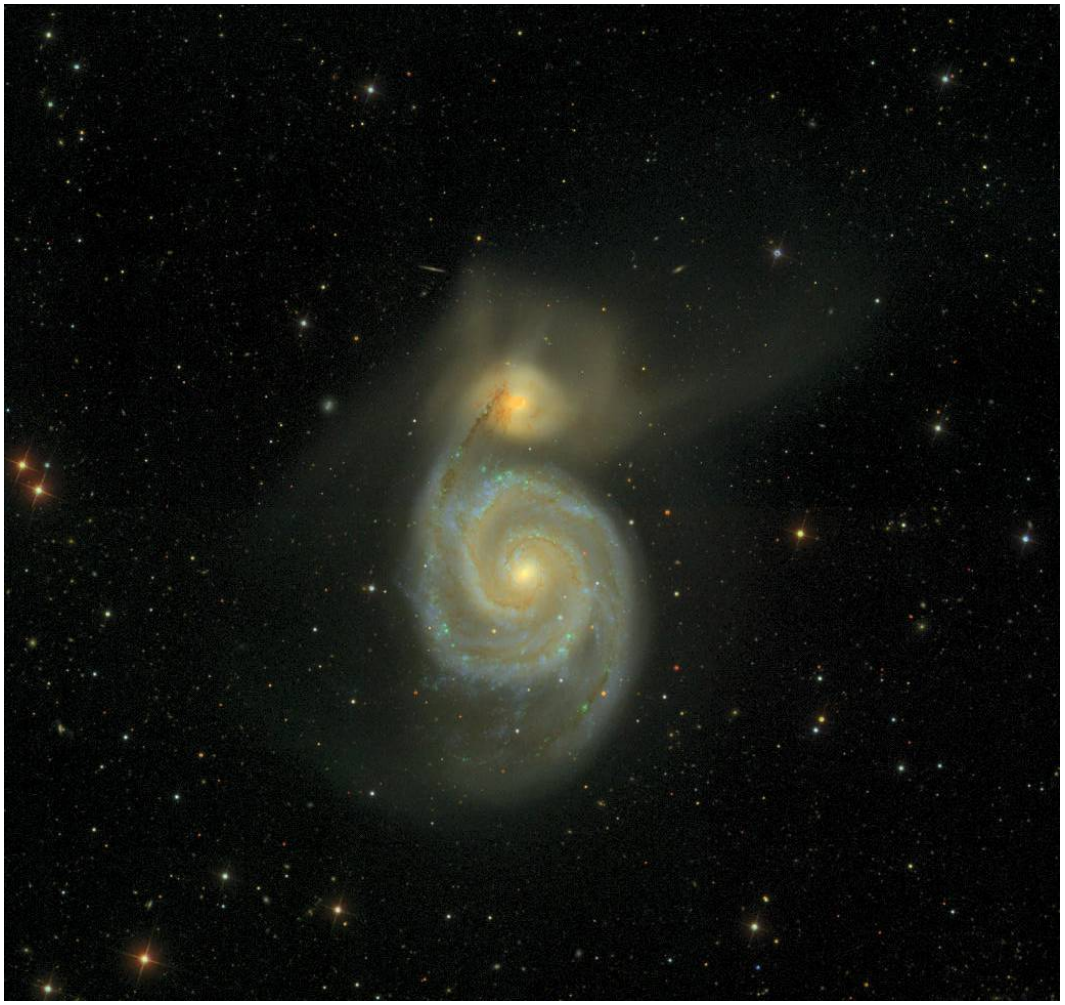

M51

model from Toomre & Toomre (1972)

at about that radius. It consists of two parts: One, of course, is the bridgelike northern arm which a number of observers (cf. Roberts and Warren 1970) have already felt partly obscures the companion. The other is the *broad*, curving, fainter counterarm to the south and southwest of the main disk. Though this second major clue is scarcely visible in the *Hubble Atlas* (Sandage 1961), it is very evident in the deeper *Sky Survey* and Arp 85 photographs and unmistakable in the IIIaJ exposure by van den Bergh (1969). Together with the projected position and excess line-of-sight velocity of the companion, it is these two features—and they alone—that comprised the prime goals of our reconstruction of the encounter shown in figures 20 and 21.

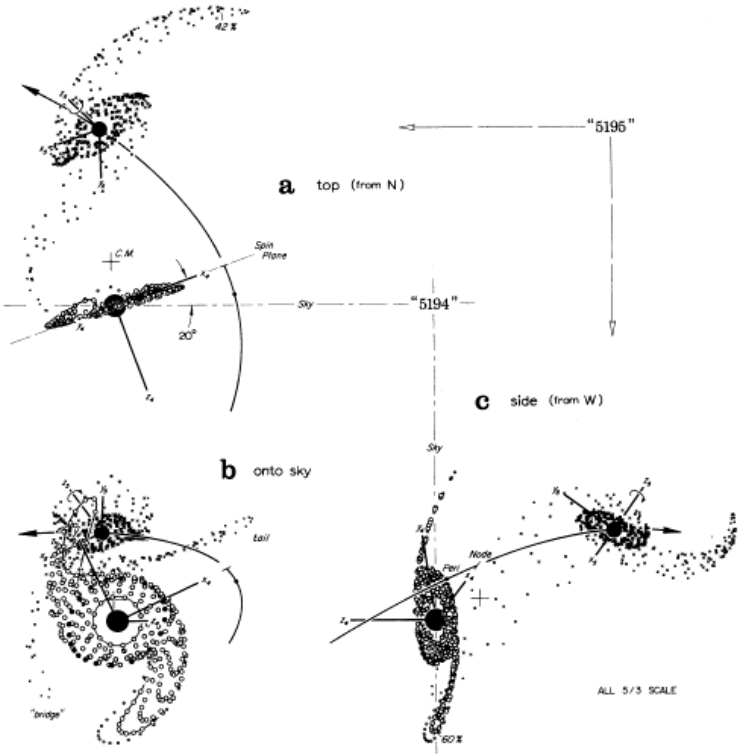

FIG. 21.—Model of the recent encounter between M51 and NGC 5195. Shown here at $t = 2.4$ are three mutually orthogonal views of the consequences of a highly elliptic $e = 0.8$ passage of a supposedly disklike "5195." This satellite was chosen to be one-third as massive, and of exactly 0.7 times the linear dimensions, of the "5194" primary—which itself contains particles from initial radii $0.2(0.05)0.4(0.033)0.633 R_{min}$. The orbit plane differs by an angle $i_4 = -70°$ from the initial spin plane of the larger disk and by $i_5 = -60°$ from that of the smaller; however, the arguments $\omega_4 = \omega_5 = -15°$ of the pericenters were here kept identical, to make the above nodal axes x_4 and x_5 exactly antiparallel. The three views show the combined system as it would appear not only (*b*) to us ($\lambda_4 = 65°$, $\beta_4 = -20°$), but also edge-on to our sky from (*a*) the "north" ($-25°$, 90°) and (*c*) the "west" (65°, 70°) directions.

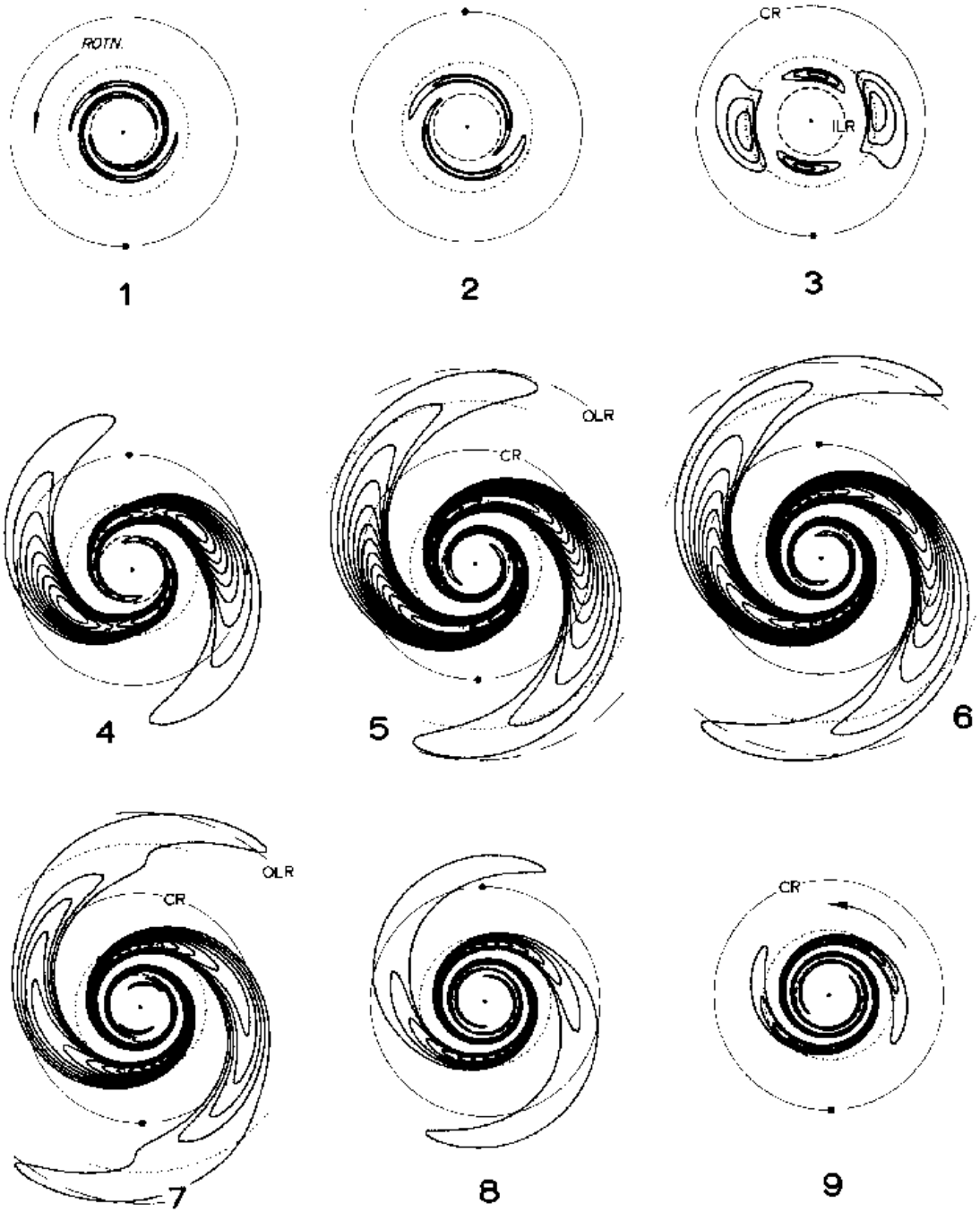

Toomre (1981)

Toomre (1981)

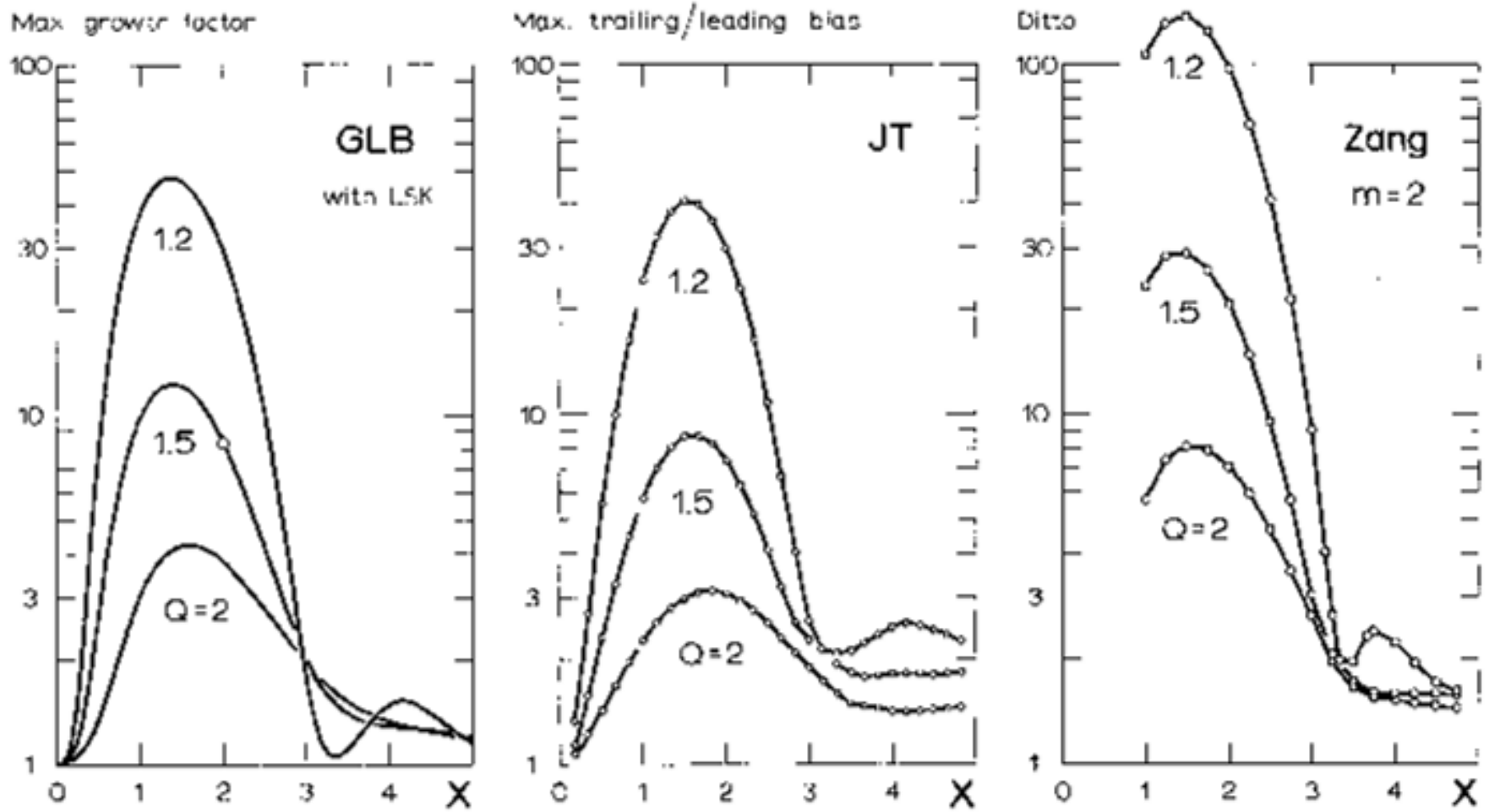
Max growth factor
GLB
with LSK
1.2
1.5
Q=2
Max. trailing/leading bias
JT
1.2
1.5
Q=2
Ditto
Zang
m=2
1.2
1.5
Q=2
100
30
10
3
1
0
1
2
3
4
X

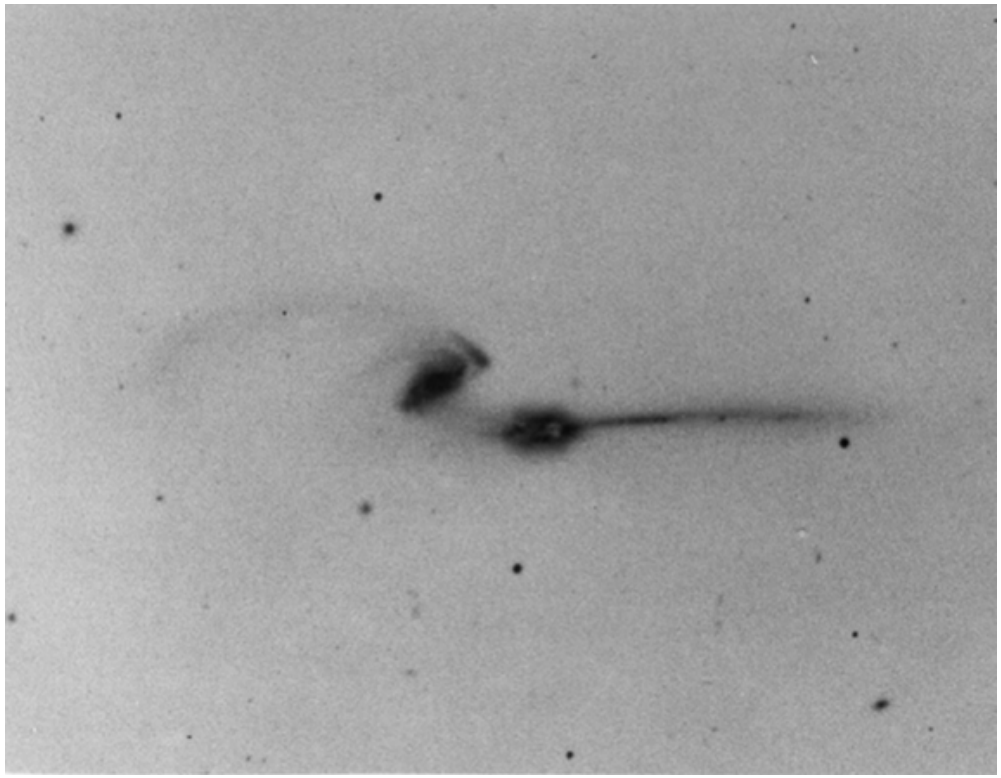

The Mice

model from Toomre & Toomre (1972)

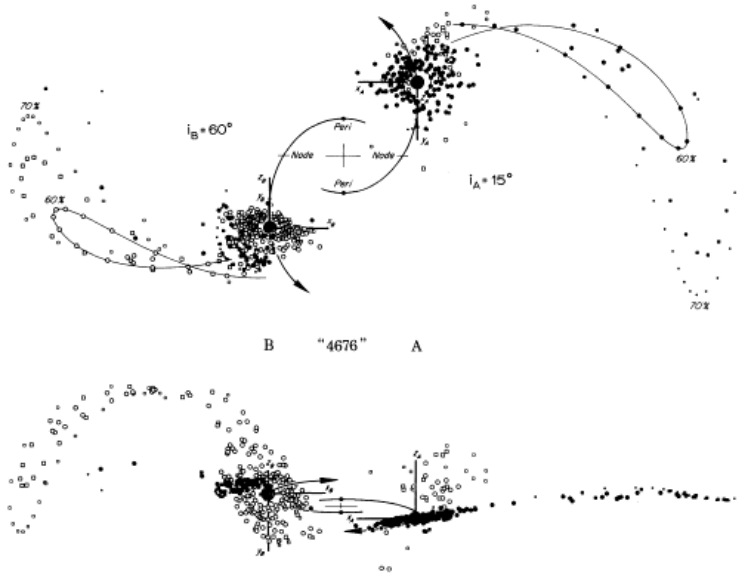

FIG. 22.—Model of NGC 4676. In this reconstruction, two equal disks of radius $0.7R_{min}$ experienced an $e = 0.6$ elliptic encounter, having begun flat and circular at the time $t = -16.4$ of the last apocenter. As viewed from either disk, the adopted node-to-peri angles $\omega_A = \omega_B = -90°$ were identical, but the inclinations differed considerably: $i_A = 15°$, $i_B = 60°$. The resulting composite object at $t = 6.086$ (cf. fig. 18) is shown projected onto the orbit plane in the upper diagram. It is viewed nearly edge-on to the same—from $\lambda_A = 180°$, $\beta_A = 85°$ or $\lambda_B = 0°$, $\beta_B = 160°$—in the lower diagram meant to simulate our actual view of that pair of galaxies. The filled and open symbols distinguish particles originally from disks A and B, respectively.

rather than elaborate, we chose the masses and loadings to be identical, did the same with the simple $\omega_A = \omega_B = -90°$, picked the round values $i_A = 15°$, $i_B = 60°$, chose the viewing longitude to be simply along the line of pericenters, and retained both the eccentricity and the 135° viewing time already used in figure 18. Thus the B object in figure 22 is virtually an "off-the-shelf" item. It differs from its predecessor in figure 18 only in the coding of certain of its particles, the display of its not-too-offensive accretion cloud above mass A, and a 45° more advanced longitude and 10° different latitude of viewing.

One almost incidental advantage of the present model is that, like the real tail A, ours looks slightly concave downward—or toward the west. More important is its agreement with the rough sense of the velocities measured in hulk B by the Burbidges: although our remnant B lacks the oval outline of the real object, its excess Doppler speeds are likewise positive and negative in the "north" and "south," respectively. (Moreover, the fact that our remnant B happens to be viewed only 20° from face-on cautions that the actual rotation in 4676B could well be twice the observed ± 200 km s^{-1}, and hence also about twice the nominal speeds of our retained test particles. Thus

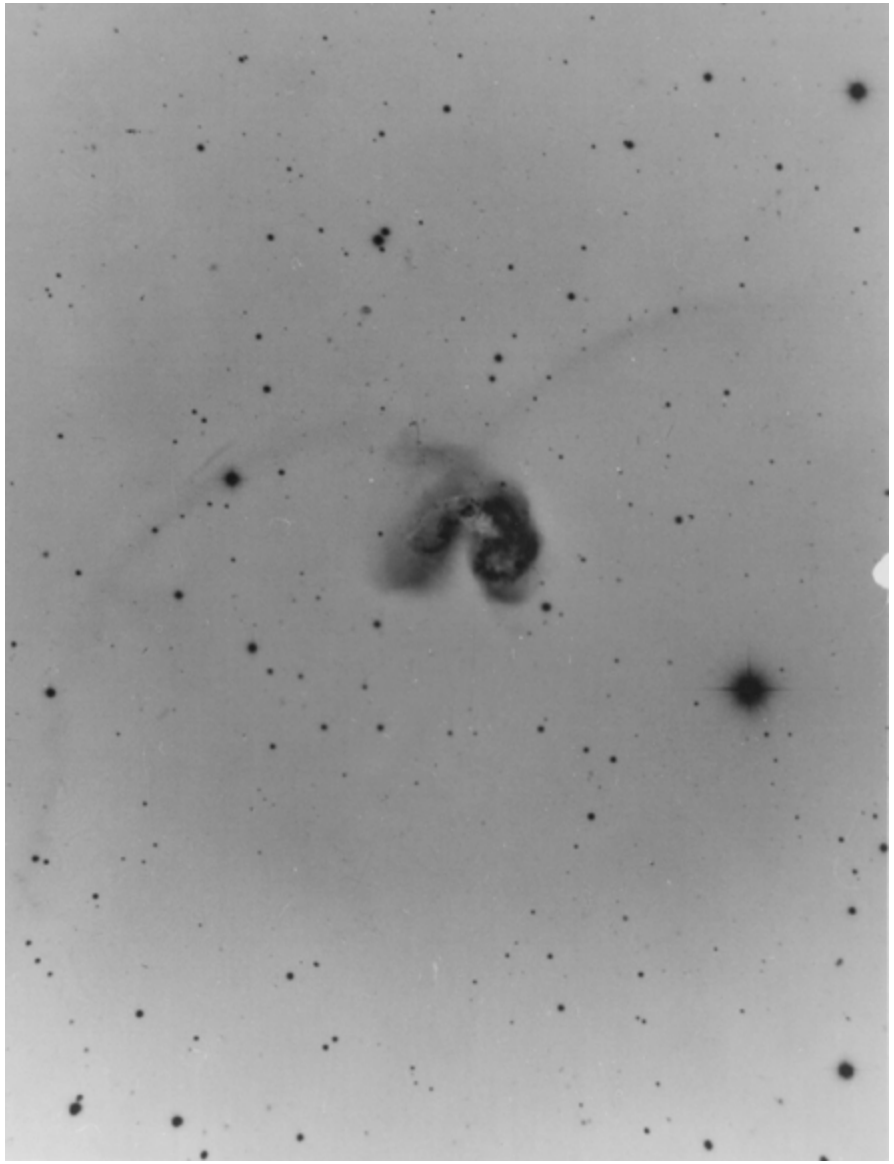

The Antennae

model from Toomre & Toomre (1972)

been concerned whether in fact it was possible to obtain seemingly *crossed* tails from tidal interactions. Figure 23 says we need not have worried.

By using figure 18, it is quite easy in retrospect to grasp the geometric essentials of this construction. Imagine that every bare companion in that ω survey carries an $i = +60°$ tail of its own, each such tail having been chosen from among the present four possibilities simply after a 180° visual rotation about the axis normal to the orbit

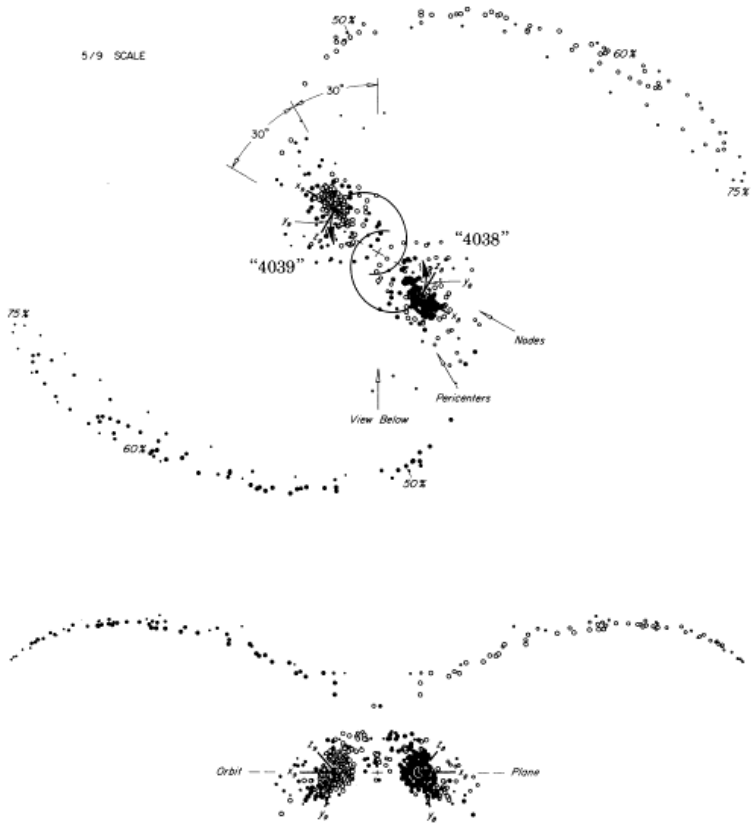

FIG. 23.—Symmetric model of NGC 4038/9. Here two identical disks of radius $0.75R_{\min}$ suffered an $e \approx 0.5$ encounter with orbit angles $i_8 = i_9 = 60°$ and $\omega_8 = \omega_9 = -30°$ that appeared the same to both. The above all-inclusive views of the debris and remnants of these disks have been drawn exactly normal and edge-on to the orbit plane; the latter viewing direction is itself 30° from the line connecting the two pericenters. The viewing time is $t = 15$, or slightly past apocenter. The filled and open symbols again disclose the original loyalties of the various test particles.

VII. BROADER ISSUES

Taken together with the pioneering work of Pfleiderer and Siedentopf—plus the recent efforts of Tashpulatov, Yabushita, and Wright—the present demonstrations should suffice as antidotes to such often-voiced sentiments as "a tidal perturbation of a galaxy can alter its shape, but cannot draw out a long narrow filament" (Gold and Hoyle 1959) or that "the bridges and tails of interacting galaxies. . . can hardly exist without a regular magnetic field" (Pikel'ner 1968).

We also suspect, however, that this work has somewhat wider implications than just that certain thin bridges or tails of a few pathological galaxies *can* indeed have arisen from violent tides. We conclude by discussing four such points, on the pretext that here, as in medicine, pathology seems instructive.

a) Eccentric Bound Orbits

Our first topic will probably seem much overdue to every thoughtful reader: Though one can certainly postulate some very close encounters on a computer, how did nearly enough of the real galaxies recently get into such a predicament?

b) Orbit Decay

Our second concern is with changes to the galactic orbits themselves as the result of an encounter. We claim almost no expertise here, since our idealized central masses obviously suffered no such changes. Yet the circumstantial evidence below seems serious enough to warrant the following questions:

When two roughly equal disk galaxies in a previously long-period orbit at last experience a close approach and raise really violent tides in each other, can it be that they also surrender a significant fraction of their orbital energy (and angular momentum) to the tail-making particles, many of which of course escape to infinity? And hence would not their remnants drop into orbits of progressively shorter periods, until at last they lose altogether their separate identities and simply blend or tumble into a single three-dimensional pile of stars?

If true, this seems a scenario for nothing less than the delayed formation of some elliptical galaxies—or at least of major stellar halos from otherwise gas-rich disks.

- peculiar galaxies arise from tides
- structure formation by gravitational instability
- mergers are common

Toomre & Toomre (1972)

c) *Stoking the Furnace?*

We have deliberately not touched earlier on the well-known tendency (e.g., Burbidge *et al.* 1963; Zwicky 1967; Arp 1969*b*, 1971*b*; Stockton 1972) of the various tails, plumes, and intergalactic bridges to involve at least one galaxy whose own color or spectrum is often unusual, or which has a high surface brightness, or which contains oddly placed absorbing material and/or emitting regions.

That such intrinsic evidence of "strangeness" has itself contributed to the reluctance to regard the external features as tidal is both clear and understandable. Nevertheless —well short of such really exotic cases as the "jets" of M87 and 3C 273—we cannot help feeling that even this share of reluctance has been somewhat excessive: Would not the violent mechanical agitation of a close tidal encounter—let alone an actual merger—already tend to bring *deep* into a galaxy a fairly *sudden* supply of fresh fuel in the form of interstellar material, either from its own outlying disk or by accretion from its partner? And in a previously gas-poor system or nucleus, would not the relatively mundane process of prolific star formation thereupon mimic much of the "activity" that is observed?

d) *Certain Exceptional Spirals?*

Lastly, we must return to those unusually fine spirals M51 and NGC 7753. As regards the former, we saw in § VI*b* that both its outer arms are plausibly tidal. Yet the same test particles showed *no* appreciable spiral structure in those deeper parts of the disk where the optical arms are most prominent, and where the recent Westerbork 21-cm continuum observations of Mathewson, van der Kruit, and Brouw (1972) and the Fabry-Perot work of Tully (1972) provide impressive support for *some* kind of a density wave—if not just the "quasi-stationary" and locally "self-sustained" spiral wave pattern first envisaged by Lin and Shu (1964, 1966) and claimed (rather vaguely) to have been corroborated for M51 by Shu, Stachnik, and Yost (1971).

In NGC 7753, where the outer structure seems again tidal, and where again one arm appears to lead to a small and *intrinsically interesting* (Arp 1969*b*) companion, the inner structure seems even better developed and more regular than in M51. Naturally one wonders in both cases if there might not be some logical connection between the outside tidal damage and the presumed waves deeper inside.

- mergers lead to starbursts
- grand-design spirals are caused by encounters

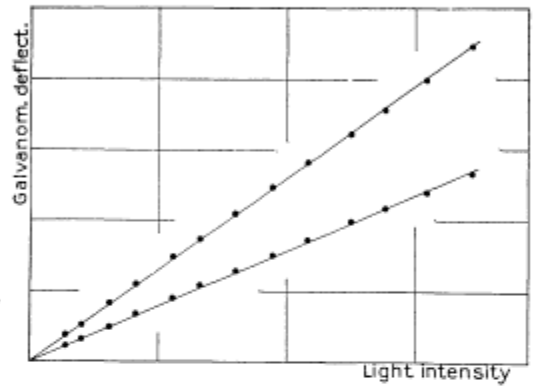

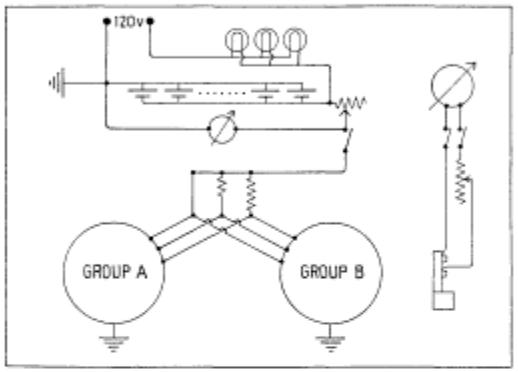

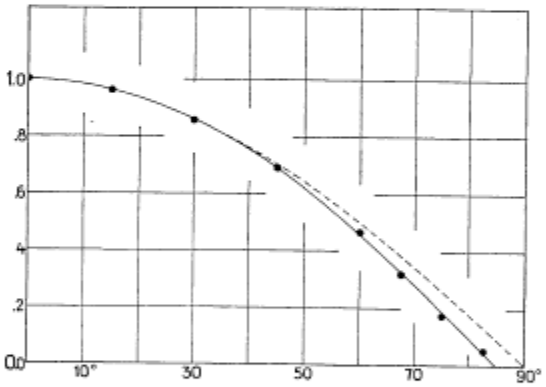

FIG. 2

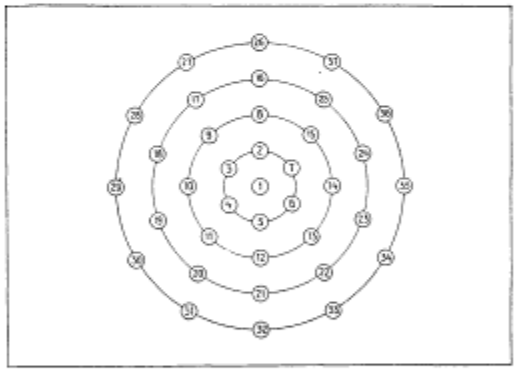

FIG. 3

FIG. 2.—(*a*) Relation between galvanometer deflection and light-intensity (resistance of 0 and 10,000 ohms). (*b*) Relation between galvanometer deflection and angle of incidence of light (*dotted line* = theoretical cosine law).

FIG. 3.—(*a*) Coupling scheme. (*b*) Arrangement of the 37 light-bulbs in groups A and B

Holmberg (1941)

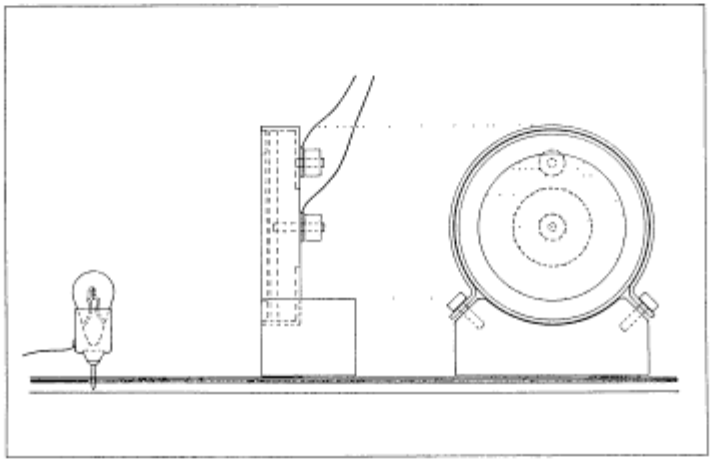

FIG. 1.—Cross-section of light-bulb and photocell (half-size)

Holmberg (1941)

FIG. 4a

FIG. 4b

FIG. 4*a*.—Tidal deformations corresponding to parabolic motions, clockwise rotations, and a distance of closest approach equal to the diameters of the nebulae. The spiral arms point in the direction of the rotation.

FIG. 4*b*.—Same as above, with the exception of counterclockwise rotations. The spiral arms point in the direction opposite to the rotation.

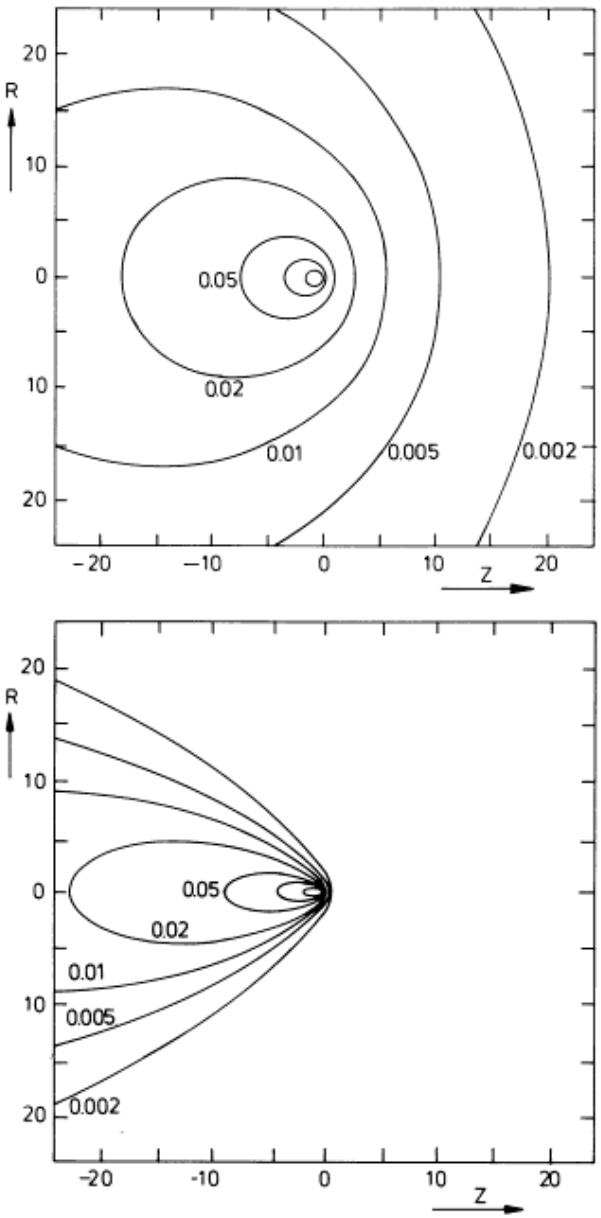

Fig. 2a and b. Response density of the medium. The extended object moves in the positive z-direction. Contours represent overdensities of 0.002, 0.005, 0.01, 0.02, 0.05, 0.1, and 0.2, using $\varrho_0 = 1$. Parameters are for **a** $v_0 = 2$, $\sigma_0 = 2$, and for **b** $v_0 = 6$ and $\sigma_0 = 2$

Mulder (1983)

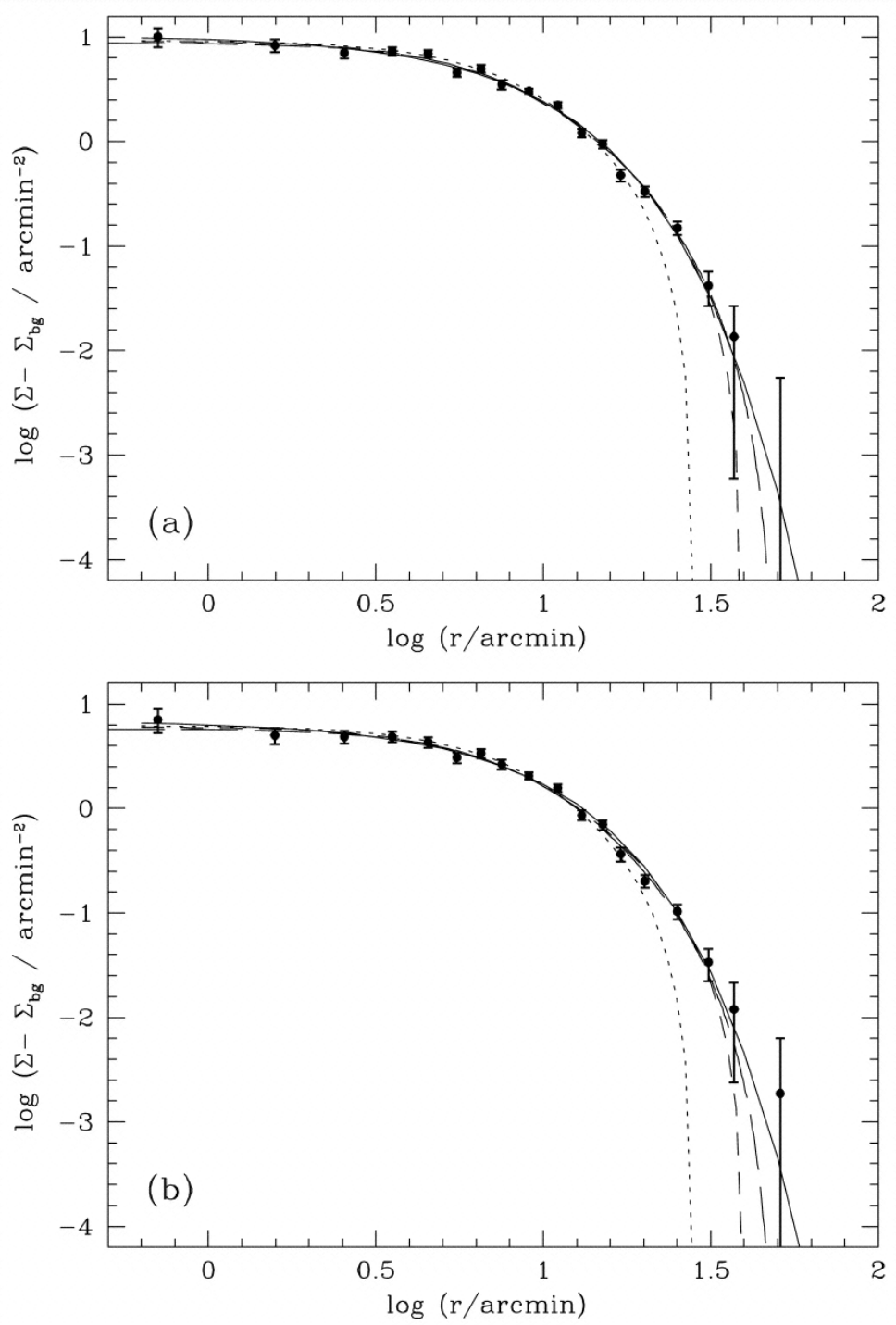

Draco dwarf spheroidal galaxy with SDSS

(Odenkirchen et al. 2001)

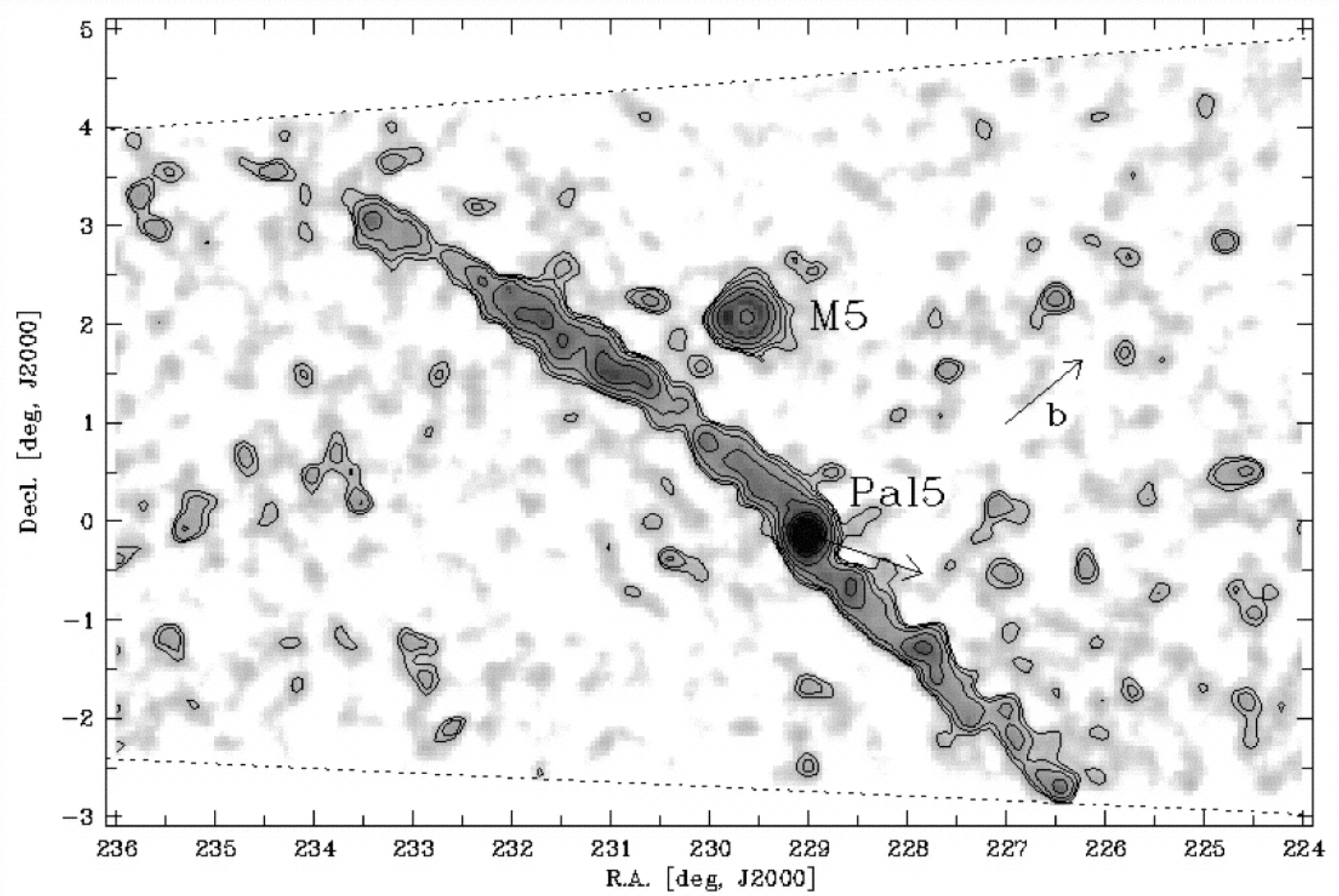

Odenkirchen et al. (2003)

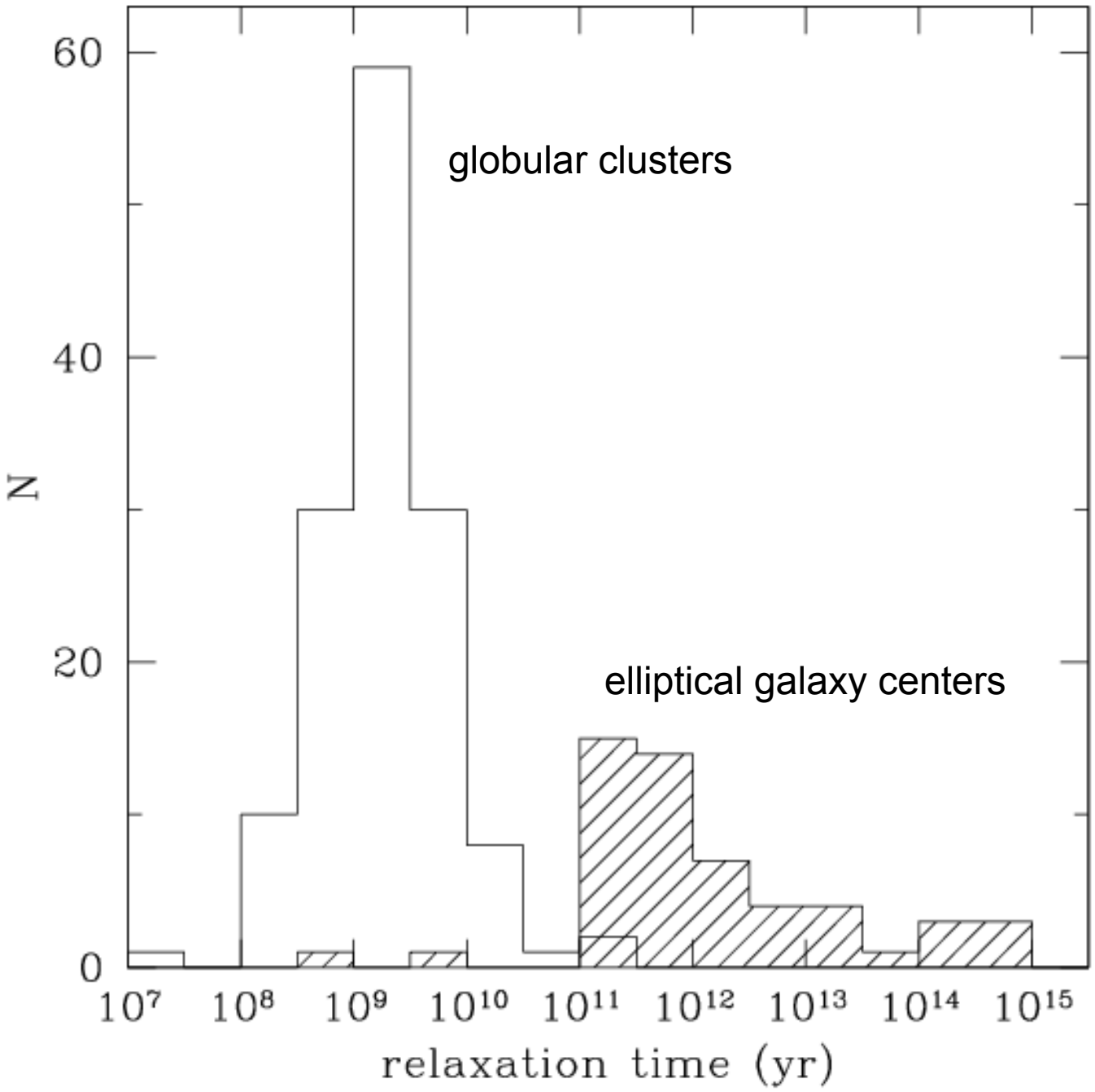
60
40
20
0
N
globular clusters
elliptical galaxy centers
10^7 10^8 10^9 10^{10} 10^{11} 10^{12} 10^{13} 10^{14} 10^{15}
relaxation time (yr)

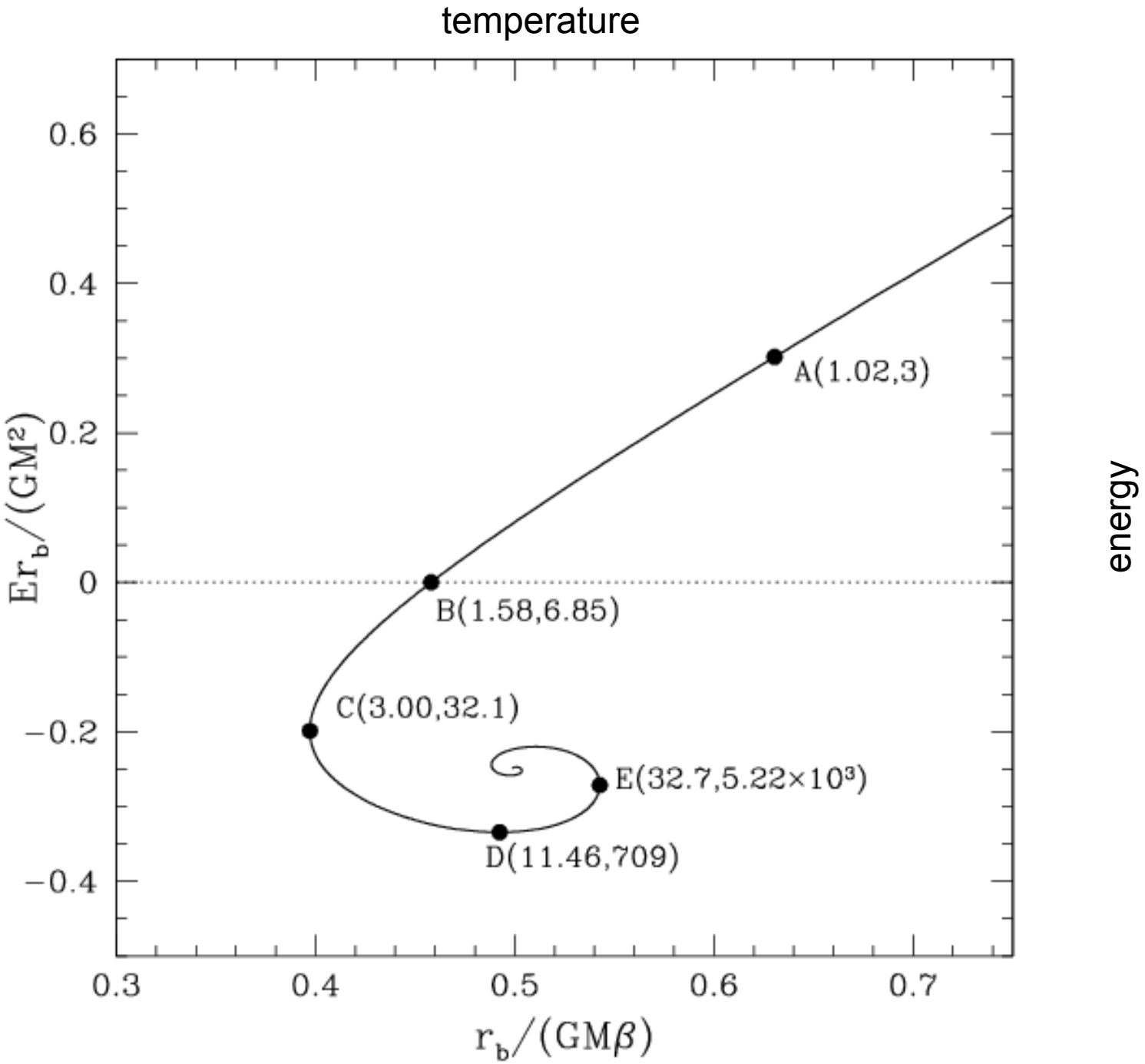
temperature
energy
0.6
0.4
0.2
0
−0.2
−0.4
0.3
0.4
0.5
0.6
0.7
$Er_b/(GM^2)$
$r_b/(GM\beta)$
A(1.02,3)
B(1.58,6.85)
C(3.00,32.1)
D(11.46,709)
E(32.7,5.22×10³)

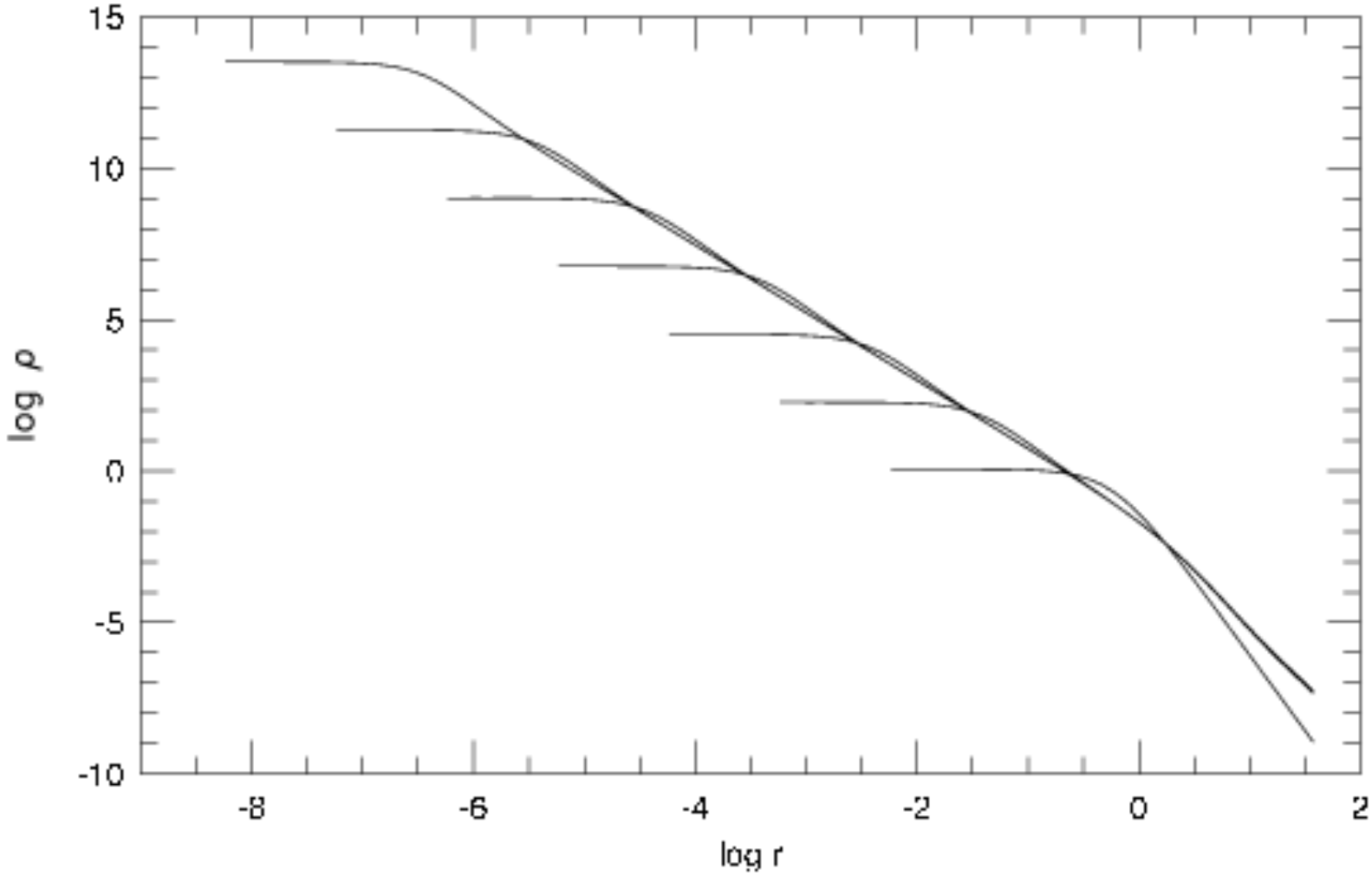

Takahashi (1995)

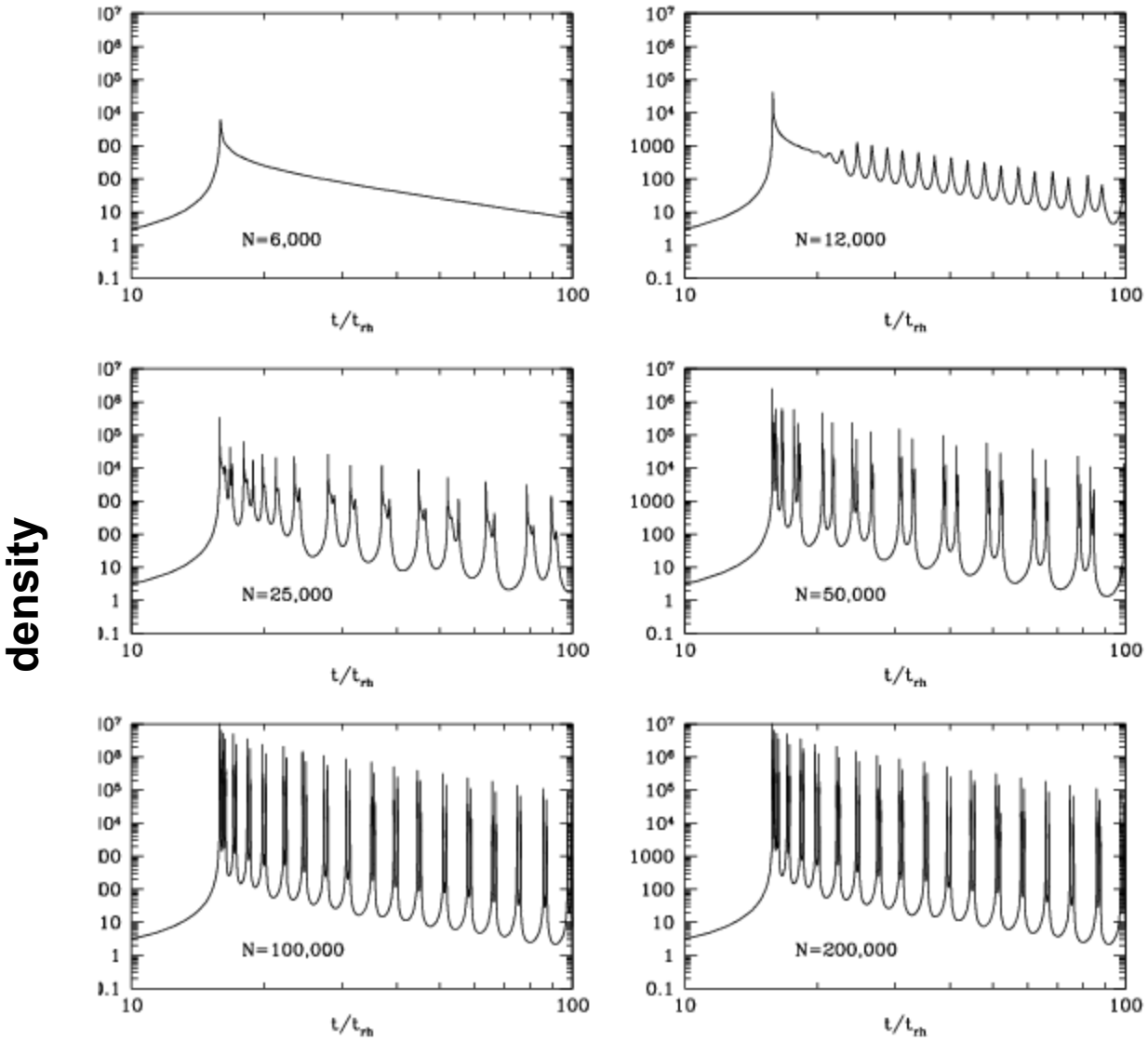

Breeden, Cohn & Hut (1994)